Study of Carbon Nanomaterials Based on Density Functional Theory

Mohammad Shafiul Alam

July 2013

Dissertation

Study of Carbon Nanomaterials Based on Density Functional Theory

Graduate School of Natural Science & Technology
Kanazawa University

Major subject: Division of Mathematical and Physical Sciences

Course: Computational Science

School registration No. 1023102010

Name: Mohammad Shafiul Alam

Chief advisor: Mineo Saito

Abstract

Carbon nanomaterials have attracted much attention because they are candidates for post-silicon materials. Since carbon nanotubes (CNTs) were detected and graphene was isolated from graphite, comprehensive studies have been carried out with the aim of exploiting the properties of these materials. In this study, by using first principles calculations, we study the interlayer distance of the two-layer graphene and atomic hydrogen adsorption in graphenes and CNTs. We first study layer distance of the two-layer graphene. We use a recently developed van der Waals density functional theory (VDWDFT) as well as the local density approximation (LDA). Both methods give successful results for graphite; i.e. the calculated interlayer distances are comparable with the experimental value. We find that the interlayer distance of the two-layer graphene is close to that of graphite. We also find that the AA stacking structure of the two-layer graphene has higher energy than that of the AB stacking one and the layer distance of the AA stacking is larger than that of the AB stacking. It is thus suggested that the interlayer distance becomes somewhat large when the stacking deviates from the AB stacking.

Next, we study hydrogen monomers and dimers in graphene, the armchair edge (5, 5) carbon nanotube (CNT), and the zigzag edge (10, 0) CNT because the presence of hydrogen atoms could change the electronic properties of graphenes and CNTs, where those hydrogen atoms are chemically attached. We find that the monomers in the above three carbon nanomaterials have the magnetic moment of 1 μ_B. In the case of the CNTs, the hydrogen atoms are located on the outer side of the CNTs. In the most stable structures of the dimers in the above three carbon materials, the two hydrogen atoms are bonded to host carbon atoms, which are nearest-neighbors. In the case of graphene, the two atoms are located on opposite sides, whereas in the

case of the armchair edge (5, 5) CNT and zigzag edge (10, 0) CNT, both hydrogen atoms are located on the outer side. The electronic structures of the most stable geometries are found to be nonmagnetic. However, when the two hydrogen atoms are bonded to second-nearest-neighbor carbon atoms, the magnetic moment is found to be 2 μ_B.

List of Publications

1. **Mohammad Shafiul Alam**, Jianbo Lin, and Mineo Saito: *First-Principles Calculation of the Interlayer Distance of the Two-Layer Graphene*: Japanese Journal of Applied Physics Vol. 50, pp 080213, August 2011.

2. **Mohammad Shafiul Alam**, Fahdzi Muttaquien, Agung Setiadi, and Mineo Saito: *First-Principles Calculations of Hydrogen Monomers and Dimers Adsorbed in Graphene and Carbon Nanotubes*: Journal of the Physical Society of Japan , vol. 82, pp: 044702, March 2013.

Dedication

Dedicated to my Mother

Contents

List of Figures

List of Tables

Chapter 1

Introduction

1.1 Carbon Nano-Material

Carbon materials have various atomic structures (fullerenes, nanotubes, graphene and graphite) as shown in Fig. 1.1. Experiments and computational simulations have been carried out for revealing of their physical properties. They have been attracting much attention for the future development of nanotechnology due to the light weight, high strength, and useful properties of semiconductors [1], metals [1], half metals [2, 3, 4], superconductors [5, 6] and magnets [7, 8, 9].

We are going to focus on carbon nanotubes (CNTs) and graphene. Since CNTs were detected from graphite [10] in 1991, is one of the carbon allotropes with sp^2 hybridization of each carbon atom. There are two kinds of CNTs, i.e; metallic CNTs and semiconducting CNTs. CNTs have a wide range of applications. Currently, CNTs can be applied in both atomistic level and macroscopic level. In the atomistic level, CNTs have been used as atomic force microscope (AFM) tip [11]. In macroscopic level, bulk CNT can be used as a composite. CNT improved the mechanical properties of cotton fiber via the coating process [12]. Beside that, CNT also has future applications. Electronic properties of the CNT can be tuned from metallic to semiconducting and vice versa. Therefore, CNTs can be used in semiconductor technology, for an example, CNT is used in a field-effect transistor as a substitute of silicon.

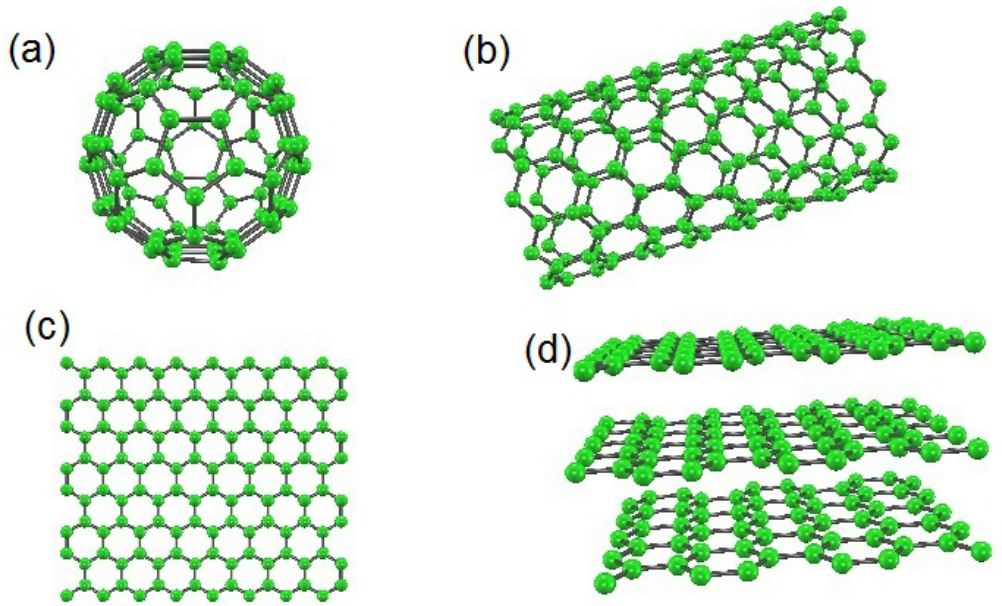

Figure 1.1: Carbon materials, (a) fullerenes, (b) nanotubes, (c) graphene and (d) graphite.

In 2004, long after the discovery of CNT, graphene [13] is isolated from graphite, a flat mono-layer of carbon atoms tightly packed into a two-dimensional hexagonal lattice. It is easier to obtain and cheaper in production. Graphene has been attracting a wide scientific interests because of novel electronic properties. Graphene does not have a band gap and there is so called Dirac cone at the zone bound points where the Fermi level is located. It has higher mobility than other semiconductor materials like silicon as well as high charge carrier concentrations, which makes graphene an interesting candidate for applications in electronic devices. The Nobel prize in Physics for 2010 was awarded to A. K. Geim and K. S. Novoselov ”for ground breaking experiments regarding the two-dimension material graphene”.

As mentioned above CNTs and graphenes are important materials for future electronic devices. In this study, we first carry out calculations of two-layer graphene to investigate layer distance. Next we focus on the calculations of atomic hydrogen adsorption in graphenes and CNTs.

1.2 Two-layer graphene layer distance

Two-layer graphene is one of the carbon materials as shown in Fig. 1.2. Nowadays, few-layer graphenes (FLG) are technologically important in semiconductor applications, due to gate control of the transport properties. Recently FLG with less than ten layers each show a distinc-

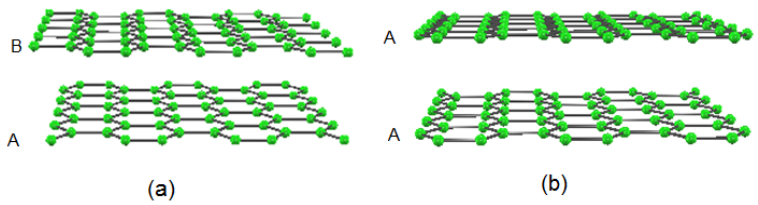

Figure 1.2: Two-layer graphene having AB stacking (a) and AA stacking (b) structures.

tive band structure [14] . There is thus an increasing interest in the physics of FLGs, with or without Bernal stacking [15, 16, 17] and their application in useful devices. The electronic properties of the few-layer graphene are different from that of the single-layer graphene and this difference raises scientific problems. In the case of the two-layer graphene, for an example, electric field opening of the band gap was theoretically predicted and experimentally confirmed [18, 19, 20, 21, 22, 23]. To study the electronic properties of few-layer graphenes, it is essential to clarify the interlayer distance but the distance is still unclear.

1.3 Atomic hydrogen adsorption

As carbon nanotubes (CNTs) were detected [10] and graphene was isolated from graphite [13], comprehensive studies have been carried out with the aim of exploiting the properties of these materials. Among a variety of applications of carbon nanostructure, hydrogen storage is considered strong candidate. Hydrogen is a common impurity in carbon materials. Hydrogen has a lower mass that makes more easily adsorbed and diffuses on the graphene layer which lower activation energies. Whereas the hydrogen molecules are physisorbed on carbon materials, hydrogen atoms are chemisorbed. Chemisorption of the hydrogen atoms to the carbon atom in graphene and CNT changes the hybridization of the carbon atoms from sp^2 to sp^3. Therefore,

this causes changing in atomic, electronic, and magnetic properties of the carbon material. This is very interesting because we could obtain materials with different properties, which consist of only hydrogen and carbon atoms. Thus, interactions between carbon material and hydrogen show great interest due to widely future applications.

Under atomic hydrogen atmospheres, hydrogen atoms are chemisorbed on graphene and CNTs [24, 25, 26, 27, 28, 29, 30, 31, 32, 33, 34, 35, 36, 37, 38, 39, 40]. Scanning tunneling microscopy and photoluminescence spectroscopy showed that some hydrogen atoms are chemically adsorbed on carbon materials [36, 37, 38, 39, 40]. Then, first-principles calculations were performed for chemisorbed hydrogen [24, 25, 26, 27, 41, 42, 43]. Duplock et al. [28] first showed that upon adsorption of hydrogen on graphene a band gap can be opened. As a result, it became clear that hydrogen significantly affects the physical properties of carbon nanomaterials. Hydrogen adsorption was found to affect the field emission of capped CNTs [44]. It is already well understood that atomic hydrogen adsorption may be a promising way to create magnetism [45, 46, 47]. This result indicated that the magnetism of carbon nanomaterials can be controlled by hydrogen chemisorption.

The electronic structure of hydrogen monomers in graphene has been well theoretically studied [24, 29, 48]. These theoretical studies showed that hydrogen is bonded to a host carbon atom and has a magnetic moment of 1 μ_B [24]. For dimers in graphene, the geometry where the two hydrogen atoms are on the same side has been studied [24, 25, 33, 34]. However, as mentioned later, we find in this study that this geometry is metastable. Details of the electronic structures, including the magnetism of the monomers and dimers in the CNTs are still unclear.

1.4 Purposes of this research

As mentioned above, in section 1.2, we discuss that the layer distance of the two-layer graphene is important in the field of carbon nanomaterials and also the nearest layer interaction is van der Waals type. Therefore, in order to investigate layer distance of the two-layer graphene VDWDFT is appropriate. Moreover, in section 1.3, we also discuss that chemisorption of

hydrogen can change in atomic, electronic and magnetic properties of carbon materials. As carbon-based materials attract much attention as candidates for the future electronic devices, we study interlayer distance of the two-layer graphene and atomic hydrogen adsorption in carbon nano-materials by simulation. Material simulation is needed to reduce of error to make a material device in the real life and also minimize enormous costs involved in any material handling project.

First we concentrate our study to find out interlayer distance of the two-layer graphene. Recently FLGs attract wide scientific interests but little is known for the interlayer distance. The interaction between the nearest layer is a van der Waals type. As we know conventional DFT (generalized gradient approximation (GGA)) is usually insufficient to include van der Waals interaction. GGA cannot be used for systems in which the vdW interaction makes a large contribution. We confirmed that GGA fails to reproduce interlayer distance. Therefore, van der Waals density functional theory (VDWDFT) is important to investigate interlayer distance of the two-layer graphene. Since layer distance is very fundamental physical quantity, we perform first-principles calculations. We employ VDWDFT and local density approximation (LDA).

Next we study atomic hydrogen adsorption on carbon nanomaterials. Hydrogenation is promising way to create magnetism. To understand the effect of hydrogen adsorption, the study of monomers and dimers is necessary since they are fundamental hydrogen impurities in carbon materials. There will be some difference between graphene and CNTs. To clarify the curvature effect, we study armchair (5, 5) edges CNT, zigzag edges(10, 0) CNT as well as graphene which is planar. The effects of hydrogenation in multi-layer graphenes are also considered. In this study, we report details of electronic structures, including magnetism of the monomers and dimers of graphenes and CNTs.

It is experimentally difficult to investigate the magnetic state in carbon nanomaterial by atomic hydrogen adsorption. Thus, this work is very important and significant in the field nanomaterials.

1.5 Structure of the thesis

In this thesis, the executional theories are explained in the Chapter 2. In the chapter 3, we reported our results by using a recently developed VDWDFT as well as the LDA. Both methods give successful results for graphite; i.e., the calculated interlayer distances are comparable with the experimental value. We find that the interlayer distance of the two-layer graphene is close to that of graphite. In Chapter 4, we report the study of hydrogen monomers and dimers in graphenes, the armchair edge (5, 5) carbon nanotube (CNT), and the zigzag edge (10, 0) CNT. We find that the monomers in the above three carbon nanomaterials have a magnetic moment of 1 μ_B. In the case of the CNTs, the hydrogen atoms are located on the outer side of the CNTs. In the most stable structures of the dimers in the above three carbon materials, the two hydrogen atoms are bonded to host carbon atoms, which are nearest-neighbors. In the case of graphene, the two atoms are located on opposite sides, whereas in the case of the armchair edge (5, 5) CNT and zigzag edge(10, 0) CNT, both hydrogen atoms are located on the outer side. However, when the two hydrogen atoms are bonded to the second nearest carbon atoms, the magnetic moment is found to be 2 μ_B. We show spin density distributions occurred by monomers and second-nearest-neighbor dimers. Finally, I summarize this work in Chapter 5.

Chapter 2

Theory and Calculational details

The results shown in this dissertation is based on the first-principles quantum-mechanical calculations. It simply says that no empirical parameters are employed in simulations to compute the electronic properties of a system, but only the atomic numbers and positions are inputs to a calculation. Due to an increase in processing power of the computer in the past few decades, it is possible to perform first-principles calculations on a larger and more realistic system. The calculations acquire a degree of accuracy, which enables direct comparison to experiments.

In this chapter, a brief overview of the theoretical methods is explained. We use the PHASE [49] calculation code. The PHASE is based on density functional theories (DFT), the pseudopotentials, and plane wave basis set. We explain the theoretical background in section 2.1. In section 2.2 density functional theory is denoted. The exchange and correlation functionals, plane wave methods, and pseodopotentials are described in sections 2.3, 2.4 and 2.5, respectively. We explain van der Waals density functional theory (VDWDFT) and calculational details in section 2.6, and 2.7, respectively.

2.1 Theoretical Background

The Hamiltonian of a fully interacting system consisting of many electrons and nuclei is expressed as:

$$\hat{H} = \hat{T_e} + \hat{T_n} + \hat{V_{ee}} + \hat{V_{nn}} + \hat{V_{ext}} \tag{2.1}$$

where $\hat{T_e}$, $\hat{T_n}$, $\hat{V_{ee}}$, $\hat{V_{nn}}$, and $\hat{V_{ext}}$ are the many electron kinetic energy operator, many-nucleus kinetic energy operator, the electron-electron interaction energy operator, many-nucleus kinetic energy operator,and the electron-nucleus interaction energy operator, respectively.

They are expressed as following:

$$\begin{cases} \hat{T_e} = -\frac{1}{2}\sum_i^N \nabla_i^2(r_i) \\ \hat{T_n} = -\frac{1}{2}\sum_j \frac{1}{M_j}\nabla_i^2(R_j) \\ \hat{V_{ee}} = \frac{1}{2}\sum_{i\neq j} \frac{1}{|\mathbf{r}_i - \mathbf{r}_j|} \\ \hat{V_{nn}} = \frac{1}{2}\sum_{i\neq j} \frac{Z_i Z_j}{|\mathbf{R}_i - \mathbf{R}_j|} \\ \hat{V_{ext}} = -\sum_{i,j} \frac{Z_j}{|\mathbf{R}_i - \mathbf{R}_j|} \end{cases} \tag{2.2}$$

where the M_i, Z_i, and $\mathbf{R_i}$ are the mass, atomic number and position of the nucleus i respectively.

The Schrödinger eigenvalue equation of this system is given by:

$$\hat{H}\Psi = E\Psi, \tag{2.3}$$

where the system wavefunction Ψ depends on all configuration variable which is expresses as:

$$\Psi = \Psi(\mathbf{r_1}, \mathbf{R_1}, \mathbf{r_2}, \mathbf{R_2}, ...). \tag{2.4}$$

This equation is defined in $3M+3N$-parameter space, and it is too complex if not impossible to solve for all but the simplest systems.

Considering the mass of a nucleus is far from that of an electron, we can assume that the motion of the nuclei is negligible compared to that of the electrons and fix their positions. By employing this, we can neglect $\hat{T_n}$ and $\hat{V_{nn}}$ and rewrite it as a problem of many electrons in an external potential $\hat{V_{ext}}$ generated by the stationary nuclei:

$$\hat{H} = \hat{T} + \hat{V_{ee}} + \hat{V_{ext}}, \tag{2.5}$$

The Schrödinger equation of this system is expressed as:

$$\hat{H}\Psi = \left[-\frac{1}{2}\sum_{i}^{N} \nabla^2 + \frac{1}{2}\sum_{i \neq j} \frac{1}{|\mathbf{r}_i - \mathbf{r}_j|} - \sum_{i,j} \frac{Z_j}{|\mathbf{R}_i - \mathbf{R}_j|} \right] \Psi = E\Psi, \tag{2.6}$$

with Ψ now the many-electron wavefunction,

$$\Psi = \Psi(\mathbf{r_1}, \mathbf{r_2}, ...). \tag{2.7}$$

This approximation method is called the **Born-Oppenheimer approximation** and is employed in all systems that are more complex than the hydrogen atom.

We know that it is possible to find the total ground state solution if we are capable of finding the ground state solutions for fixed nuclear configurations, our problem is reduced to finding these electronic ground state solutions. For this, it is useful to introduce some additional approximations, such as variation principle and Hartree-Fock approximation. Before we explain Hartree-Fock approximation, first we discuss the variation principle.

2.1.1 The variation Principle

To find any eigenfunction of the Hamiltonian operator is an impossible task, but we may consider all the (many-body) eigenfunctions ϕ_i were known. Assuming that the set of these eigenfunctions is complete, we may expand any other wavefunctions ψ of the system with the same number of electrons. We, therefore, write down the following expansion.

$$|\Psi\rangle = \sum_i c_i |\phi_i\rangle \tag{2.8}$$

where c_i are the expansion coefficients. The eigenstates $|\phi_i\rangle$ are assumed to be orthonormal. The wavefuntion is assume to be normalized, then the expectation value for the energy of the wavefunction is given by:

$$E = \langle\Psi|\hat{H}|\Psi\rangle = \sum_{i,j} c_j^* c_i \langle\phi_i|\hat{H}|\phi_j\rangle = \sum_i |c_i^2| E_i \geq E_0 \sum_i |c_i^2| = E_0 \tag{2.9}$$

with E_0 the lowest eigenvalue of $\hat{H}$, i.e. the ground state energy. The expectation value of the energy of any wavefunction ψ is thus higher than or equal to the ground state energy. This result is very important as this allows us to search for the ground state wavefunction and energy by testing different 'trial wavefunctions'. It also accepts the state corresponding to the lowest energy as the best approximation of the true ground state.

Now the problem is to find out a good trial wavefunctions. In practice, the approximate wavefunction is written in terms of one or more parameters:

$$\Psi = \Psi(p_1, p_2, ..., p_N) \tag{2.10}$$

So, the expectation value for the energy, E, is a function of these parameters and can be minimized with respect to them by requiring that

$$\frac{\partial E(p_1, p_2, ..., p_N)}{\partial p_1} = \frac{\partial E(p_1, p_2, ..., p_N)}{\partial p_2} = ... = \frac{\partial E(p_1, p_2, ..., p_N)}{\partial p_n} = 0 \tag{2.11}$$

Let us assume that the approximate wavefunction for a given system may be expanded in terms of a particular set of plane waves. Because we cannot work with an infinitely many numbers of plane waves, we truncate the sum and just consider the first N terms:

$$\phi = \sum_{j}^{N} c_j \exp(-i\mathbf{k} \cdot \mathbf{r_j}) \tag{2.12}$$

In order to get a good approximation ground state, we would like the above expansion to satisfy the minimum condition, i.e:

$$\frac{\partial}{\partial c_j^*} \frac{\langle \phi | \hat{H} | \phi \rangle}{\langle \phi | \phi \rangle} = 0 \tag{2.13}$$

for each c_j. In addition, we require the approximate wavefunction to remain normalized:

$$\langle \phi | \phi \rangle = 1 \tag{2.14}$$

which then we can rewrite Eq.(2.13) as:

$$\frac{\partial}{\partial c_j^*} \langle \phi | \hat{H} | \phi \rangle = 0 \tag{2.15}$$

for all c_j. We can satisfy Eq.(2.14) and Eq.(2.15) by introducing a new quantity which is expressed as:

$$K = \langle\phi|\hat{H}|\phi\rangle - \lambda\left[\langle\phi|\phi\rangle - 1\right] \tag{2.16}$$

and extending the minimization property to include extra parameter λ,

$$\frac{\partial K}{\partial c_j^*} = \frac{\partial K}{\partial \lambda} = 0 \tag{2.17}$$

here λ is called the *Lagrange multipliers*. Inserting the expansion in Eq.(2.12) into Eq.(2.17), we get

$$\sum_j c_j \left(\langle exp(-i\mathbf{k}\cdot\mathbf{r_i})|\hat{H}|exp(-i\mathbf{k}\cdot\mathbf{r_j})\rangle - \lambda\langle exp(-i\mathbf{k}\cdot\mathbf{r_i})|exp(-i\mathbf{k}\cdot\mathbf{r_j})\rangle\right) = 0 \tag{2.18}$$

We can write in the form of a generalized eigenvalue equation,

$$\sum_j H_{ij}c_j = \lambda\delta_{ij} \tag{2.19}$$

where $H_{ij} = \langle exp(-i\mathbf{k}\cdot\mathbf{r_i})|\hat{H}|exp(-i\mathbf{k}\cdot\mathbf{r_j})\rangle$ and $\delta_{ij} = \langle exp(-i\mathbf{k}\cdot\mathbf{r_i})|exp(-i\mathbf{k}\cdot\mathbf{r_j})\rangle$. We can solve these N equations ($i = 1, 2, ...N$) by calculating the matrix element H_{kj} and δ_{ij}. If we use N basis functions to expand the trial function ϕ, Eq.(2.12) then gives N eigenvalues. By multiplying Eq.(2.18) with c_i^* and summing over i we get the following expression;

$$\lambda = \frac{\sum_{i,j} c_i^* c_j \langle exp(-i\mathbf{k}\cdot\mathbf{r_i})|\hat{H}|exp(-i\mathbf{k}\cdot\mathbf{r_j})\rangle}{\sum_{i,j} c_i^* c_j \langle exp(-i\mathbf{k}\cdot\mathbf{r_i})|exp(-i\mathbf{k}\cdot\mathbf{r_j})\rangle} \tag{2.20}$$

Eq. (2.20) implies that each of the N eigenvectors correspond to a series of expansion coefficients yielding different ϕ and each λ corresponds to a different expectation value. The eigenvector corresponds to the smallest eigenvalue then corresponds to the best ϕ and the smallest eigenvalue itself is the closest approximation to the ground state energy.

2.1.2 The Hartree-Fock approximation

A major problem with trying to solve the many-body Schrödinger equation is the representation of the many-body wavefunction. In 1920, Douglas Hartree [50] developed an approach named after himself called the Hartree approximation. He simplified the problem of electron-electron

interactions by expanding the many electron wavefunction into a product of single electron wavefunction which is capable of solving the multi-electron Schrödinger equation of the wavefunction. With this hypothesis and the use of the **variation principle**, need to be solved N equations for an N single electrons system, with wavefunction, $\Psi(\mathbf{r_i})$:

$$\Psi_H(\mathbf{r_1}, \mathbf{r_2}, \mathbf{r_3}, ...\mathbf{r_N}) = \frac{1}{\sqrt{N}}\phi(\mathbf{r_1}), \phi(\mathbf{r_2}), \phi(\mathbf{r_3}), ...\phi(\mathbf{r_N}) \tag{2.21}$$

where $\Psi(\mathbf{r_i})$ is composed of spatial wavefunction $\phi(\mathbf{r_i})$.

However, the Hartree approximation does not account for exchange interaction as Eq.(2.21) does not satisfy **Pauli's exclusion principle**. According to **Pauli's exclusion principle** it is known that Hartree approximation fails as the Hartree product wavefunction is symmetric not antisymmetric.

We need to establish such as a reasonable approximation which has good physical meaning. Hartree and Fock introduce an approximation method that deals with electrons as distinguish particle. In the Hartree-Fock scheme, the system with N-electron wave function is approximated by *antisymmetric* function.

The Hartree-Fock scheme is always described as *Slater Determinant* such as:

$$\Psi_{HF} = \frac{1}{\sqrt{N!}} \begin{vmatrix} \phi_1(\mathbf{r_1}) & \phi_2(\mathbf{r_1}) & \cdots & \phi_{N/2}(\mathbf{r_1}) \\ \phi_1(\mathbf{r_2}) & \phi_2(\mathbf{r_2}) & \cdots & \phi_{N/2}(\mathbf{r_2}) \\ \vdots & \vdots & \cdots & \vdots \\ \phi_1(\mathbf{r_N}) & \phi_2(\mathbf{r_N}) & \cdots & \phi_{N/2}(\mathbf{r_N}) \end{vmatrix} \tag{2.22}$$

or in short:

$$\Psi_{HF} = \frac{1}{\sqrt{N!}} det\left|(\mathbf{r_1})\phi_2(\mathbf{r_2}).....\phi_{N/2}(\mathbf{r_N})\right| \tag{2.23}$$

with additional orthonormal constraint

$$\int \phi_i^*(\mathbf{r})\phi_i(\mathbf{r})d\mathbf{r} = \langle\phi_i|\phi_j\rangle = \delta_{ij} \tag{2.24}$$

With the above Slater Determinant, we can be determined the HF energy by taking the expectation value of the Hamitonian Eq.(2.6). It can be expressed by the given equation:

$$E = \langle\Psi_{HF}|\hat{H}|\Psi_{HF}\rangle = 2\sum_i^{N/2} h_i + \sum_i^{N/2}\sum_j^{N/2}(2J_{i,j} - K_{i,j}) \tag{2.25}$$

the first term of the Eq. (2.25) indicates the kinetic energy of electrons and interaction between electrons-nuclei, then the second term represents the interaction between two electrons called Coulomb and exchange integrals, where: where

$$h_i = \int \phi_i^*(\mathbf{r_1})\hat{h}\phi_i(\mathbf{r_1})d\mathbf{r_1} \tag{2.26}$$

$$\mathbf{J_{ij}} = \int\int \phi_i^*(\mathbf{r_1})\phi_i(\mathbf{r_1})\frac{1}{|\mathbf{r_1}-\mathbf{r_2}|}\phi_j^*(\mathbf{r_2})\phi_j(\mathbf{r_2})d\mathbf{r_1}d\mathbf{r_2} \tag{2.27}$$

$$\mathbf{K_{ij}} = \int\int \phi_i^*(\mathbf{r_1})\phi_j(\mathbf{r_1})\frac{1}{|\mathbf{r_1}-\mathbf{r_2}|}\phi_j^*(\mathbf{r_2})\phi_i(\mathbf{r_2})d\mathbf{r_1}d\mathbf{r_2} \tag{2.28}$$

The term $\mathbf{J_{ij}}$ are called Coulomb integrals, which are already present in the Hartree Approximation. On the other hand, the exchange integral $\mathbf{K_{ij}}$ are represented something new. Mention that it is not necessary to exclude the term $i = j$ from the double summation in equation Eq. (2.25), it is because $J_{ij} = K_{ij}$.

In order to understand in a simple way about Coulomb and exchange in Eq. 2.25, we consider V_{HF} as Hartree-Fock potential. This potential describes the repulsive interaction between one electron with others N-1 electrons averagely, consists Coulomb operator $\hat{J}$ and exchange operator $\hat{K}$.

$$\hat{J}\phi(\mathbf{r}) = \int d\mathbf{r_2}\frac{|\phi_j(\mathbf{r_2})|^2}{|\mathbf{r_1}-\mathbf{r_2}|}\phi_i(\mathbf{r_1}) \tag{2.29}$$

$$\hat{K}\phi(\mathbf{r}) = \int d\mathbf{r_2}\frac{\phi_j^*(\mathbf{r_2})\phi_i(\mathbf{r_2})}{|\mathbf{r_1}-\mathbf{r_2}|}\phi_j(\mathbf{r_1}) \tag{2.30}$$

In the Eq. (2.29) is called the $\hat{J}$ is called the coulomb operator. In order to understand the meaning of the Coulomb operator, suppose we have two electrons in different positions $\mathbf{r_1}$ and $\mathbf{r_2}$ in such spin orbital ϕ_i. These electrons will repel each other, which in Hartree-Fock scheme. The repulsive force of the first electron due to second electron is weighted by the possibility of the existence of the second electron itself at this spatial point. This Coulomb operator is called *local* as its expectation value only depends on the spin orbital at $\mathbf{r_1}$.

The term $\hat{K}$in the Eq.(2.30) is defined exchange operator. This operator comes out to avoid the self-interaction in one electron. Of course, this is an important point as it is meaningless if we had to calculate the Coulomb interaction between one electron with itself. We may call exchange operator as non local because the result of the exchange operator on an orbital, ϕ_i, depends on the ϕ_i at every point in space. It is an important point that the non-local exchange operator $\hat{K}$ highlighted when we operate its with spin orbital, ie.ϕ_i on spin: By putting $\phi_i(\mathbf{r}) = \phi_i(\mathbf{r}, \sigma)$ in Eq. (2.30) we can find that the exchange interaction only affects electrons with like spins. The Hartree-Fock theory reduces the energy expectation value as electrons of like spin are kept apart. The exchange energy is the difference between the Hartree and Hartree-Fock values.

The Hartree-Fock theory does nothing to keep electrons with opposite spin away. Such electrons can interact only through the average charge density appearing in coulomb operator. There is no pairing interaction to make it disagreeable for electrons of opposite side come together. This suggests that the ground-state energy calculated in Hartree-Fock theory is always higher than the true ground-state energy $E_{HF} > E_0$.

The Hartree-Fock scheme is constructed based on the effective wavefunction and potential. We guess the first set input of Slater determinant based on Pauli's principle for the system, so we have reasonable approximation wave function. Then we construct the potential operator with emphasizing the electron's interaction that taken account averagely and considering the self-interaction in one electron. Next iteration is done based on the new orbitals from previous calculation until we reach the threshold point. This technique is also known as *self-consistent field* (SCF).

2.2 Density Functional Theory (DFT)

The Hartree-Fock equations deal with exchange exactly; however, the equations neglect more detailed correlations due to many-body interactions. The effects of electronic correlations are not negligible. The requirement for a computationally practicable scheme that successfully

incorporates the effects of both exchange and correlation leads us to consider the conceptually disarmingly simple and elegant density functional theory(DFT). Nowadays, DFT is an efficient and practical method to describe ground state properties of materials due to high computational efficiency and good accuracy. The idea of DFT is to describe interacting system via electron's density, not wave functions. DFT is totally based on two theorems stated by Hohenberg and Kohn [51]. Here we explain the two theorems as following:

2.2.1 Hohenberg-Kohn Theorems

There are two important theorems that can be resumed from Hohenberg-Kohn work. The theorems support us for determining the Hamiltonian operator, and the properties of the system based on electron density point of view. The electronic density $n(\mathbf{r})$ is expressed as:

$$n(\mathbf{r}) = \mathbf{N} \sum_{\mathbf{s_1}} ... \sum_{\mathbf{s_N}} \int ... \int |\mathbf{\Psi}(\mathbf{r}, \mathbf{s_1}, \mathbf{r_2}, \mathbf{s_2}, ...\mathbf{r_N}, \mathbf{s_N})|^{\mathbf{2}} \mathbf{dr_2}.....\mathbf{dr_N} \tag{2.31}$$

$$\int n(\mathbf{r}) d\mathbf{r} = N \tag{2.32}$$

Theorem I. (Hohenberg-Kohn 1, 1964) *The ground state density $n(\mathbf{r})$ of a many-body quantum system in some external potential $V_{ext}(\mathbf{r})$ determines this potential uniquely.*

Proof: Hohenberg-Kohn proved the first theorem by *reducio ad absurdum*. They assumed another external potential, $V'_{ext}(\mathbf{r})$, that differed by a constant from first external potential but give rise to the same density $n(\mathbf{r})$. Now, we have two Hamiltonian operator, $\hat{H}$ and $\hat{H}'$, that give corresponding ground wave function (Ψ and Ψ') and energies (E_0 and E'_0). Obviously; these two ground state energies are different. This condition gives us a chance to use the Ψ' for calculating the expectation value of $\hat{H}$:

$$E_0 < \langle \Psi' | \hat{H} | \Psi' \rangle = \langle \Psi' | \hat{H}' | \Psi' \rangle + \langle \Psi' | \hat{H} - \hat{H}' | \Psi' \rangle \tag{2.33}$$

As the value of Hamiltonian are: $\hat{H} = \hat{T} + \hat{V}_{ee} + \hat{V}_{ext}$ and $\hat{H} = \hat{T} + \hat{V}_{ee} + \hat{V}'_{ext}$. We can get:

$$E_0 < E'_0 + \int n(\mathbf{r})[V_{ext} - V'_{ext}] d\mathbf{r} \tag{2.34}$$

and (by changing the quantities)

$$E_0' < E_0 + \int n(\mathbf{r})[V_{ext} - V_{ext}']d\mathbf{r} \tag{2.35}$$

Then we add the Eq. (2.34) and Eq. (2.35), this summation will lead to inconsistency:

$$E_0 + E_0' < E_0 + E_0' \tag{2.36}$$

Thus the theorem proved by *reductio ad absurdum*

Theorem II. (Hohenberg-Kohn 2, 1964) *A universal functional for the energy $E[n]$ in terms of the density $n(\mathbf{r})$ can be defined, valid for any external potential $V_{ext}(\mathbf{r})$. For any particular $V_{ext}(\mathbf{r})$, the exact ground state energy of the system is the global minimum value of this functional, and the density $n(\mathbf{r})$ that minimizes the functional is the exact ground state density $n_0(\mathbf{r})$.*

Proof: Since all properties such as the kinetic energy, etc., are uniquely determined if $n(\mathbf{r})$ is specified, then each such property can be viewed as a functional of $n(\mathbf{r})$, including the total energy functional:

$$\begin{aligned} E_{HK}[n(\mathbf{r})] &= T[n] + E_{int}[n] + \int v_{ext}(\mathbf{r})n(\mathbf{r})d^3\mathbf{r} + E_{II} \\ &= F[n(\mathbf{r})] + \int v_{ext}(\mathbf{r})n(\mathbf{r})d^3\mathbf{r} + E_{II} \end{aligned} \tag{2.37}$$

where E_{II} is the interaction energy of nuclei and $F[n(\mathbf{r})]$ is a universal functional of the charge density $n(\mathbf{r})$ because the treatment of the kinetic and internal potential energies are the same for all systems. In the ground state, the energy is defined by the unique ground state density, $n^{(1)}(\mathbf{r})$,

$$E_0 = E[n^{(1)}] = \langle\Psi|\hat{H}|\Psi\rangle \tag{2.38}$$

By the variational principle, a different density, $n^{(2)}\mathbf{r})$ will necessarily give a higher energy:

$$E_0 = E[n^{(1)}] = \langle\Psi|\hat{H}|\Psi\rangle < \langle\Psi'|\hat{H}|\Psi'\rangle = E_0^{'} \tag{2.39}$$

It follows that minimizing with respect to $n(\mathbf{r})$ the total energy of the system written as a functional of $n(\mathbf{r})$, one finds the total energy of the ground state. The correct density that

minimizes the energy is then the ground state density. In this way, DFT exactly reduce the N-body problem to the determination of a 3-dimensional function $n(\mathbf{r})$ which minimize the functional $E_{HK}[n(\mathbf{r})]$. But unfortunately this is of little use as $E_{HK}[n(\mathbf{r})]$ is not known.

2.2.2 The Kohn-Sham equations

Kohn-Sham reformulated the problem in a more familiar form and opened the way to practical applications of DFT. They continued to prove the theorem which states that the total energy of the system depends only on the electron density of the system [52].

$$E = E[n(\mathbf{r})] \tag{2.40}$$

An interacting electrons system is mapped in an auxiliary system of a non-interacting electrons with the same ground state charge density $n(r)$.For a system of non-interacting electrons the ground-state charge density is represented as a sum over one-electron orbitals.

$$n(\mathbf{r}) = 2\sum_{i}^{N} |\Psi_i(\mathbf{r})|^2, \tag{2.41}$$

where i runs from 1 to $N/2$ if we consider double occupancy of all states.

The electron density n(**r**) can be varied by changing the wave function $\Psi(\mathbf{r})$ of the system. If the electron density n(**r**) corresponds to the said wavefunction, then its total energy is the minimized energy, and the whole system is in a ground state. The Kohn-Sham approach is to replace interacting electron, which is difficult with non-interacting electrons, which move in an effective potential [52]. The effective potential consists the external potential, and Coulomb interaction between electrons, and its effect such as exchange and correlation interactions. By solving the equations, we can get ground state density and energy. The accuracy of the solution is limited to the approximation of exchange and correlation interactions. It is convenient to write Kohn-Sham energy functional for the ground state including external potential is:

$$E_{KS} \;=\; T_s[n(\mathbf{r})] + E_H[n(\mathbf{r})] + E_{XC}[n(\mathbf{r})] + \int d\mathbf{r} V_{ext}(\mathbf{r}) n(\mathbf{r}) \tag{2.42}$$

The first term is the kinetic energy of non-interacting electrons:

$$T_s[n(\mathbf{r})] = -\frac{\hbar^2}{2m} 2 \sum_i \int \Psi_i^*(\mathbf{r}) \nabla^2 \Psi_i^*(\mathbf{r}) d\mathbf{r} \tag{2.43}$$

The second term (called the Hartree energy) contains the electrostatic interaction between cloud of charge:

$$E_H[n(\mathbf{r})] = \frac{e^2}{2}\int \frac{n(\mathbf{r})n(\mathbf{r}')}{|\mathbf{r}-\mathbf{r}'|}d\mathbf{r}d\mathbf{r}' \tag{2.44}$$

All effects of exchange and correlation are grouped into exchange-correlation energy E_{XC}. If all the functional $E_{XC}[n(\mathbf{r})]$ were known, we could obtain exact ground state density and energy of the many body problem.

Kohn-Sham energy problem is a minimization problem with respect of the density $n(\mathbf{r})$. Solution of this problem can be obtained by using functional derivative as below

$$\begin{aligned}\frac{\delta E_{KS}}{\delta\Psi_i^*(\mathbf{r})} &= \frac{\delta T[n]}{\delta\Psi_i^*(\mathbf{r})} + \left[\frac{\delta E_{ext}[n]}{\delta n(\mathbf{r})} + \frac{\delta E_H[n]}{\delta n(\mathbf{r})} + \frac{\delta E_{XC}[n]}{\delta n(\mathbf{r})}\right]\frac{\delta n(\mathbf{r})}{\delta\Psi_i^*(\mathbf{r})} \\ &\quad -\frac{\delta\left(\lambda\left(\int n(\mathbf{r})d\mathbf{r}-N\right)\right)}{\delta n(\mathbf{r})}\left[\frac{\delta n(\mathbf{r})}{\delta\Psi_i^*(\mathbf{r})}\right] = 0,\end{aligned} \tag{2.45}$$

where λ is Lagrange multiplier and The exchange-correlation potential, V_{XC}, is given formally by the functional derivative

$$V_{XC} = \frac{\delta E_{XC}[n]}{\delta n(\mathbf{r})} \tag{2.46}$$

$$\frac{\delta n(\mathbf{r})}{\delta\Psi_i^*(\mathbf{r})} = \Psi_i(\mathbf{r}),$$

the last term is Lagrange multiplier for handling the constraints, so we can get non-trivial solution.

The first, second, and third terms of eq. (2.45) are

$$\frac{\delta T[n]}{\delta\Psi_i^*(\mathbf{r})} = -\frac{\hbar^2}{2m}2\nabla^2\Psi_i(\mathbf{r}) \tag{2.47}$$

$$\begin{aligned}\left[\frac{\delta E_{ext}[n]}{\delta n(\mathbf{r})} + \frac{\delta E_H[n]}{\delta n(\mathbf{r})} + \frac{\delta E_{XC}[n]}{\delta n(\mathbf{r})}\right]\frac{\delta n(\mathbf{r})}{\delta\Psi_i^*(\mathbf{r})} &= 2(V_{ext}(\mathbf{r}) + V_H(\mathbf{r}) + V_{XC}(\mathbf{r}))\Psi_i(\mathbf{r}), \\ \frac{\delta\left(\lambda\left(\int n(\mathbf{r})d\mathbf{r}-N\right)\right)}{\delta n(\mathbf{r})}\left[\frac{\delta n(\mathbf{r})}{\delta\Psi_i^*(\mathbf{r})}\right] &= 2\varepsilon_i\Psi_i(\mathbf{r})\end{aligned} \tag{2.48}$$

Inserting eq. (2.47), and (2.48) to eq. (2.45), we can obtain Kohn-Sham equation which satisfies many body Schrödinger equation.

$$\left(-\frac{1}{2}\nabla^2 + V_{KS}(\mathbf{r})\right)\Psi_i(\mathbf{r}) = \varepsilon_i\Psi_i(\mathbf{r}) \tag{2.49}$$

where

$$V_{KS}(\mathbf{r}) = V_{ext}(\mathbf{r}) + V_H(\mathbf{r}) + V_{XC}(\mathbf{r}) \tag{2.50}$$

or,

$$V_{KS}(\mathbf{r}) = V_{ext}(\mathbf{r}) + \frac{e^2}{2}\int \frac{n(\mathbf{r}')}{|\mathbf{r}-\mathbf{r}'|}d\mathbf{r}' + V_{XC}(\mathbf{r}) \tag{2.51}$$

If the virtual independent-particle system has the same ground state as the real interacting system, then the many-electron problem reduces to one electron problem. Thus we can write:

$$V_{KS}(\mathbf{r}) = V_{eff}(\mathbf{r}) \tag{2.52}$$

The kinetic energy $T_s[n(\mathbf{r})]$ is given by

$$T_s[n(\mathbf{r})] = \sum_i \varepsilon_i - \int n(\mathbf{r})V_{eff}(\mathbf{r})d\mathbf{r} \tag{2.53}$$

By substituting this formula in equation 2.42, the total energy is given by as follows:

$$E_{KS}[n(\mathbf{r})] = \sum_i \varepsilon_i + \frac{1}{2}\int\int \frac{n(\mathbf{r})n(\mathbf{r}')}{|\mathbf{r}-\mathbf{r}'|}d\mathbf{r}d\mathbf{r}' + E_{xc}[n] - \int n(\mathbf{r})V_{eff}(\mathbf{r}))d\mathbf{r} \tag{2.54}$$

Since the Hartree term and V_{xc} depend on $n(\mathbf{r})$, which depend on Ψ_i, the problem of solving the Kohn-Sham equation has to be done in a self-consistent (iterative) way. Usually one starts with an initial guess for $n(\mathbf{r})$, then calculates the corresponding V_H and V_{xc} solves the Kohn-Sham equations for the Ψ_i . From this one calculates a new density and starts again. This procedure is then repeated until convergence is reached (Fig. 2.1)

2.3 Exchange and Correlation Functional

The major problem with DFT is that the exact functionals for exchange and correlation are not known except for the free-electron gas. In previous section, the many body problems are

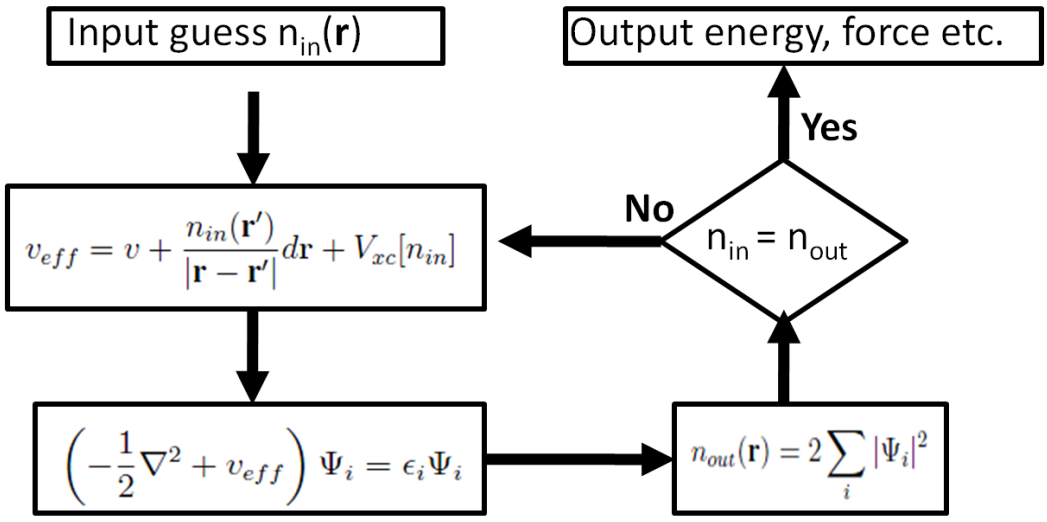

Figure 2.1: Self-consistent scheme of Kohn-Sham equation

rewritten to the effective one-electron problem by using the Kohn-Sham equation. But, the Kohn-Sham equation cannot be solved since the derivative $E_{XC}[n(\mathbf{r})]$ is not known. Therefore, it is very important to have an accurate XC energy functional $E_{XC}[n(\mathbf{r})]$ or potential $V_{XC}(\mathbf{r})$ in order to give a satisfactory description of a realistic condensed-matter system. For a homogeneous electron gas, this will only depend on the value of the electron density. For a non-homogeneous system, the value of the exchange correlation potential at the point $\mathbf{r}$ depend not only on the value of density at $\mathbf{r}$, but also the variation close to $\mathbf{r}$.

2.3.1 Local Density Approximation (LDA)

As the functional $E_{XC}[n(\mathbf{r})]$ is unknown one has to find a good approximation for it. A simple approximation, which was already suggested by Hohenberg and Kohn, is the LDA or in the spin polarized case the local-spin-density approximation (LSDA). The exchange-correlation energy per particle by its homogeneous electron gas (HEG) $e_{XC}[n(\mathbf{r})]$ is expressed by:

$$\begin{aligned} E_{xc}^{LDA}[n(\mathbf{r})] &= \int n(\mathbf{r}) e_{xc}^{homo}(n(\mathbf{r}))d\mathbf{r} \\ &= \int n(\mathbf{r}) \left[e_x^{homo}(n(\mathbf{r})) + e_c^{homo}(n(\mathbf{r}))\right] d\mathbf{r} \end{aligned} \tag{2.55}$$

for spin polarized system

$$E_{xc}^{LSDA}[n_+(\mathbf{r}), n_-(\mathbf{r})] = \int n(\mathbf{r}) e_{xc}^{homo}(n_+(\mathbf{r}), (n_-(\mathbf{r}))d\mathbf{r} \tag{2.56}$$

The exchange energy $e_x(n(\mathbf{r}))$ is

$$e_x^{LDA}(n(\mathbf{r})) = -\frac{3}{4\pi}k_f \tag{2.57}$$

where the Fermi wavevector $k_f = (3\pi^2 n)^{\frac{1}{3}}$.

The expression of the correlation energy density of the HEG at high density limit has the form:

$$e_c = Aln(r_s) + B + r_s(Cln(r_s) + D) \tag{2.58}$$

and the density limit takes the form

$$e_c = \frac{1}{2}\left(\frac{g_0}{r_s} + \frac{g_1}{r_s^{3/2}} + ...\right) \tag{2.59}$$

where where the Wigner-Seitz radius r_s is related to the density as

$$r_s = (3/(4\pi n))^{\frac{1}{3}} \tag{2.60}$$

For spin polarized systems, the exchange energy functional is known exactly from the result of spin-unpolarized functional:

$$E_x[n_+(\mathbf{r}), n_-(\mathbf{r})] = \frac{1}{2}(E_x[2n_+(\mathbf{r})] + E_x[2n_-(\mathbf{r})]) \tag{2.61}$$

The spin-dependence of the correlation energy density is approached by the relative spin-polarization:

$$\xi(\mathbf{r}) = \frac{n_+(\mathbf{r}) - n_-(\mathbf{r})}{n_+(\mathbf{r})n_-(\mathbf{r})} \tag{2.62}$$

The spin correlation energy density $e_c(n(\mathbf{r}), \xi(\mathbf{r})$ is so constructed to interpolate extreme values $\xi = 0, \pm 1$, corresponding to spin-unpolarized and ferromagnetic situations. The XC potential $V_{XC}(n(\mathbf{r}))$ in LDA is given by:

$$\frac{\delta E_{XC}[n]}{\delta n(\mathbf{r})} = \int d\mathbf{r}\left[\epsilon_{xc} + n\frac{\partial \epsilon_{xc}}{\partial n}\right] \tag{2.63}$$

$$V_{XC}(\mathbf{r}) = \epsilon_{xc} + n\frac{\partial \epsilon_{xc}}{\partial n}, \tag{2.64}$$

$$E_{XC}[n] = \int d\mathbf{r} n(\mathbf{r}) \epsilon_{xc}([n], \mathbf{r}), \tag{2.65}$$

where $\epsilon_{xc}([n], \mathbf{r})$ is the energy per electron that depends only on the density $n(\mathbf{r})$.

The LDA sometimes allows useful predictions of electron densities, atomic positions, and vibration frequencies. However, The LDA also makes some errors: total energies of atoms are less realistic than those of HF approximation, and binding energies are overestimated. LDA also systematically underestimates the band gap.

2.3.2 Generalized Gradient Approximation (GGA)

The density of electron is not always homogeneous as we expected. In the case of inhomogeneous density, naturally, we have to carry out the expansion of electronic density in the term of gradient and higher order derivatives, and they are usually termed as generalized gradient approximation (GGA). GGAs are still local but also take into account the gradient of the density at the same coordinate. Three most widely used GGAs are the forms proposed by Becke [53] (B88) , Perdew et al. [54, 55], and Perdew, Burke and Enzerhof [56] (PBE). The definition of the exchange-correlation energy functional of GGA is the generalized form in Eq. (2.56)to include corrections from density gradient $\nabla n(\mathbf{r})$ as :

$$E_{xc}^{GGA}[n_+(\mathbf{r}), n_-(\mathbf{r})] = \int n(\mathbf{r}) e_{xc}[n(\mathbf{r}) F_{XC}[n(\mathbf{r}), |\nabla n_+(\mathbf{r})|, |\nabla n_-(\mathbf{r})|, ...] d\mathbf{r} \tag{2.66}$$

Here, F_{XC} is the escalation factor that modifies the local density approximation (LDA) expression according to the variation of density in the vicinity of the considered point, and it is dimensionless [57]. The exchange energy expansion will introduce a term that proportional to the squared gradient of the density. If we considered up to fourth order, the similar term also appears proportional to the square of the density's Laplacian. Recently, the general derivation of the exchange gradient expansion has been up to sixth order by using second order density response theory [58]. The lowest order (fourth order) terms in the expansion of F_x have been calculated analytically [58, 59]. This term is given by the following:

$$F_X(m, n) = 1 + \frac{10}{81} m + \frac{146}{2025} m^2 - \frac{73}{405} nm + Dm^2 + O(\nabla \rho^6) \tag{2.67}$$

where

$$m = \frac{|\nabla\rho|^2}{4(3\pi^2)^{2/3}\rho^{8/3}} \tag{2.68}$$

is the square of the reduced density gradient, and

$$n = \frac{\nabla^2\rho}{4(3\pi^2)^{2/3}\rho^{5/3}} \tag{2.69}$$

is the reduced Laplacian of density.

These are the comparison of GGAs with LDA (LSDA)

1. It enhances the binding energies and atomic energies,
2. It enhances the bond length and bond angles,
3. It enhances the energetics, geometries, and dynamical properties of water, ice, and water clusters,
4. Semiconductors are marginally better described within the LDA than in GGA, except for binding energies,
5. For *4d-5d* transition metals, the improvement of GGA over LDA is not clear, depends on how well the LDA does in each particular case,
6. Lattice constant of noble metals (Ag, Au, and Pt) are overestimated in GGA, and
7. There is some improvement in the gap energy; however, it is not substantial as this feature related to the description of the screening of the exchange hole when one electron is removed, and this point is not taken into account by GGA.

2.4 Plane Waves Method

Plane wave methods are much more efficient than all-electron ones to calculate the atomic forces and hence to determine the equilibrium geometries. Plane waves are not centered at the nuclei but extend throughout the complete space. They implicitly involve the concept of

periodic boundary condition. Therefore, they enjoy great popularity in solid state physics for which they are particularly adopted. The Kohn-Sham equation can be described by using plane waves. As the arrangement of the atoms within the cell is periodic in the real space, so the wave functions must satisfy Bloch's theorem, which can be written by:

$$\Psi_i(\mathbf{r}) = \exp(\mathbf{ik} \cdot \mathbf{r})\mathbf{u_k}(\mathbf{r}), \tag{2.70}$$

where $u_k(\mathbf{r})$ is periodic in space with the same periodicity with the cell which can be expanded into a set of plane waves

$$u_i(\mathbf{r}) = \sum_{\mathbf{G}} c_{i,\mathbf{G}} exp(i\mathbf{G} \cdot \mathbf{r}) \tag{2.71}$$

Combining eq. (2.70) and (2.71, each electronic wave function can be expressed as

$$\Psi_i(\mathbf{r}) = \sum_{\mathbf{G}} c_{i,\mathbf{k+G}} exp(i(\mathbf{k} + \mathbf{G}) \cdot \mathbf{r}) \tag{2.72}$$

Kohn-Sham equation in eq. (2.49) is substitute in terms of reciprocal space **k** as below:

$$\sum_{\mathbf{G'}} \left[\frac{1}{2} |\mathbf{k+G}|^2 \delta_{G,G'} + V_{KS}(\mathbf{G\text{-}G'}) \right] c_{i,\mathbf{k+G}} = \varepsilon_i c_{i,\mathbf{k+G}} \tag{2.73}$$

Solution of the Kohn-Sham equation can be obtained by diagonalization of the Hamiltonian matrix. The diagonal part is the kinetic term, otherwise are the potential term. To limit the summation over **G**, cut off energy is applied to the kinetic term which is expressed by

$$E_{cut} = \frac{1}{2} |\mathbf{k+G}|^2 \equiv \mathbf{G}_{cut}^2 \tag{2.74}$$

The limitation of the energy is reasonable due to the fact that lower energy is more important.

2.5 Pseudopotential

The maximum number of plane waves is required to expand the tightly bonded core electrons due to rapid oscillation near the nuclei. However, valence electrons greatly affect far more than the core electrons of the electron structure of the material. The concept of a pseudopotential is

the replacement of one problem with another. The primary application in electronic structure is to replace the strong Coulomb potential of the nucleus and the effects of the tightly bound core electrons by an effective ionic potential acting on the valence electrons. A pseudopotential can be generated in an atomic calculation and then used to compute properties of valence electrons in molecules or solids, since the core states remain almost unchanged. Furthermore, the fact that pseudopotential are not unique allows the freedom to choose from that simplify the calculations and the interpretation of the resulting electron structure. There are two types of famous pseudopotential, norm conserving pseudopotential and ultrasoft pseudopotential

2.5.1 Norm Conserving Pseudopotential

In this kind of pseudopotential, there are some requirements to be fulfilled [60]. Those requirements are

1. All the electrons and pseudo valence eigenvalues are the same as the selected atomic configuration.

$$\epsilon_i^{AE} = \epsilon_i^{PS} \tag{2.75}$$

2. All the electrons and pseudo valence eigenvalues are in agreement in an external core region.

$$\Psi_i^{AE}(r) = \Psi_i^{PS}(r), \quad r \geq R_c \tag{2.76}$$

3. The logarithmic derivatives and their first energy derivative of real and pseudo wavefunctions match at the cut-off radius R_c.

$$\frac{d}{dr} \ln \Psi_i^{AE}(r) = \frac{d}{dr} \ln \Psi_i^{PS}(r) \tag{2.77}$$

4. The total charge inside core radius R_c for each wave function must be same (norm conservation).

$$\int_0^{R_c} dr |\Psi_i^{AE}(r)|^2 = \int_0^{R_c} dr |\Psi_i^{PS}(r)|^2 \tag{2.78}$$

5. The first energy derivative of the logarithmic derivatives of all-electron and pseudo wave functions must be same for $r \geq R_c$. This condition is implied by point 4.

2.5.2 Ultrasoft Pseudopotential

This pseudopotential releases norm conservation criteria to obtain smoother pseudo wave functions [61]. The pseudo wave functions are divided into two parts:

1. Ultrasoft valence wave functions which omit norm conservation criteria ϕ_i^{US}.

2. A core augmentation charge.

$$Q_{nm}(r) = \Psi_n^{AE*}(r)\Psi_m^{AE}(r) - \Psi_n^{US*}(r)\Psi_m^{US}(r) \tag{2.79}$$

The ultrasoft pseudopotential takes the form of

$$V^{US} = V_{loc}(r) - \sum_{nmI} D_{nm}^0 |\beta_n^I\rangle\langle\beta_m^I| \tag{2.80}$$

where β is projector function which is expressed by

$$|\beta_n\rangle = \sum_m \frac{|X_m\rangle}{\langle X_m|\phi_n\rangle} \tag{2.81}$$

and they are strictly localized inside the cut-off region for the wave functions since the X - functions are defined through

$$|X_n\rangle = (\epsilon_n - \hat{T} - V_{loc})|\phi_n\rangle \tag{2.82}$$

$$D_{nm}^0 = \langle\phi_n\rangle|X_m\rangle + \epsilon_m q_{nm} \tag{2.83}$$

The scattering properties of the pseudopotential can be improved by using more than one β projector function per angular momentum channel.

It is necessary to use generalized eigen value formalism. For this case we introduce the overlap operator S

$$\hat{S} = \mathbf{1} + \sum_{nmI} q_{nm}|\beta_n^I\rangle\langle\beta_m^I| \tag{2.84}$$

where

$$q_{nm} = \int_0^{r_c} dr Q_{nm}(r) \tag{2.85}$$

Then the charge density is expressed by

$$\begin{aligned} n(\mathbf{r}) &= \sum_i \phi_i^*(r)\hat{S}\phi_i(r) \\ &= \sum_i \left[|\phi_i(\mathbf{r})|^2 + \sum_{nmI} Q_{nm}^I(\mathbf{r}) \langle \phi_i | \beta_n^I \rangle \langle \beta_m^I | \phi_i \rangle \right], \end{aligned} \tag{2.86}$$

2.6 van der Waals density functional theory (VDWDFT)

We employ van der Waals density functional theory [62, 63] VDWDFT) to investigate the layer distance of two-layer graphene. In chapter 3, in the VDWDFT, we first perform self-consistent calculation where only the GGA exchange potential is included in the many body potential. Next we evaluate the total energy by using the following exchange-correlation energy:

$$E_{xc}^{vdW-DF} = E_{ex}^{GGA} + E_c^{LDA} + E_c^{nl}, \tag{2.87}$$

where E_{xc}^{vdW-DF} , E_{ex}^{GGA}, and E_c^{LDA} are the exchange-correlation energy in the VDWDFT, GGA exchange energy, and the LDA correlation energy, respectively. E_c^{nl} is the nonlocal correlation energy which is expressed as

$$E_c^{nl} = \frac{1}{2} \int d\mathbf{r}_i d\mathbf{r}_k \rho(\mathbf{r}_i) \phi(\mathbf{r}_i, \mathbf{r}_k) \rho(\mathbf{r}_k), \tag{2.88}$$

where $\phi(\mathbf{r}_i, \mathbf{r}_k)$ is a nonlocal function and ρ is the electron density obtained from the above mentioned self-consistence calculation.In appendix **A**, we will discuss details about VDWDFT.

2.7 Calculation details

In chapter **3**, we use the following method and conditions. In the calculation of graphite, we use the rectangular lattice in which four atoms in each layer are contained. The maximum kinetic energy of the plane waves is 36 rydberg and $10 \times 10 \times 10$ k-point mesh in the full

Brillouin zone (BZ) is used. In the calculation of the two-layer graphene, we use the repeated slab model where the length of the the vacuum region is 10.58 Å and the k-point mesh in the full Brillouin zone is $10 \times 10 \times 1$. We apply the least square fourth or fifth order polynomials fitting to the function of the total energy over the interlayer distance. Based on the result of this fitting, We determine the equilibrium interlayer distance and the interlayer binding energy (ϵ) which is the difference between the energies for the equilibrium layer distance and the infinite layer one.

In chapter 4, we use the calculation method which is in details as follows: We perform spin-polarized GGA calculations by using PHASE software [49] in which the plane wave basis set and pseudopotentials are used. The maximum kinetic energies of the plane waves and the charge densities are 340 eV (25 Rydberg) and 3128 eV (230 Rydberg), respectively.

In the calculation of graphene, we use a repeated slab model where the spacing of the slab is 6.71 Å, which is equal to the lattice constant of the c-axis of the graphite. When we increase the spacing of the slab up to 10 Å, the binding energy variation of the hydrogen dimer is less than 10 meV. The two-dimensional supercell size is 17.04 $\times$ 19.68 Å^2 and this supercell contains 128 carbon atoms. The 2×2 k-point mesh in the two-dimensional Brillouin zone (BZ) is used. When we increase the numbers of k-points to 8×8, the binding energy variation of the hydrogen dimer is only 20 meV.

We also study the armchair edge (5,5) CNT and zigzag edge (10,0) CNT, which have diameters of 7.1 and 7.9 Å, respectively. The one-dimensional cell lengths of the armchair edge (5,5) CNT and zigzag edge (10,0) CNT are 13.2 and 11.6 Å, respectively. The supercells of these CNTs contain 120 carbon atoms. The k-point mesh in the one-dimensional BZ is 2. When we increase the number of k-points to 8, the binding energy variation of the hydrogen dimer is only 40 meV.

Based on the result of the calculations, we determine the binding energy per hydrogen atom E_b of the C-H bond, which is defined as [64]

$$E_b = \frac{E(system) + n_H E_{at}(H) - E_t(hydrogenated\ system)}{n_H}, \tag{2.89}$$

where $E(system)$ is the total energy of the pristine system and $E_t(hydrogenated\ system)$ is

that of the hydrogenated system. $E_{at}(H)$ is the energy of a single hydrogen atom and n_H is the number of hydrogen atoms in the hydrogenated system. In the calculation of $E_{at}(H)$, the same corresponding unit cells of graphene and the CNTs are used.

Chapter 3

Layer distance of the two-layer graphene

In this chapter, we study interlayer distance of the two-layer graphene. Recently, few-layer graphenes are technologically important in semiconductor applications, due to gate control of the transport properties. The electronic properties of the few-layer graphene are different from that of the single-layer graphene and this difference raises scientific problems. In the case of the two-layer graphene, for an example, electric field opening of the band gap was theoretically predicted and experimentally confirmed [18, 19, 20, 21, 22, 23]. To study the electronic properties of few-layer graphenes, it is essential to clarify the interlayer distance but the distance is still unclear. It was reported from high resolution transmission electron microscopy (TEM) observation that interlayer distances of double-layer graphitic carbon systems are up to 3.84 Å, [65] and inter shell distances of multiwalled carbon nanotubes are in the range from 3.59 to 3.62 Å [66]. These observed distances are larger than the interlayer distance of graphite (3.35 Å). First principles calculations based on the generalized gradient approximation (GGA) indicated that the interlayer distance of the two-layer graphene is larger than that of graphite [67]. This result seems to be consistent with the above mentioned experimental results. However, the interaction between the nearest layer is a van der Waals type, so the validity of the GGA is unclear. Conventional DFT (local density approximation (LDA) and GGA) is usually insufficient to include van der Waals interaction, which is prominent in weakly bonded materials such as molecular crystal and many organic compounds [68, 69, 70].

In this study, we perform first principles calculations based on the LDA, GGA and van der Waals density functional theory (VDWDFT) [62, 63]. We find that the interlayer distance of the two-layer graphene is close to that of graphite. We also find that the metastable AA stacking structure has larger interlayer distance than that of the AB stacking structure. Therefore, the deviation from the AB stacking is expected to enlarge the interlayer distance.

3.1 Results and Discussions

We first carry out LDA calculations of graphite having the AB stacking structure. Our calculated interlayer distance is 3.35 Å; therefore, our calculation well reproduce the experimental value (3.35 Å) [71]. We note that our calculated value is comparable with a previous calculation based on the LDA (3.33 Å [72]. The energy of the AB stacking structure is 11.0 meV/atom lower than that of the AA stacking structure (Table 3.1). The interlayer distance (3.60 Å) of the AA stacking structure is larger than the corresponding value of the AB stacking structure (3.35 Å). Our results for the graphite are consistent with those of the past LDA calculations, i.e., it was also shown that the AB stacking structure has a lower energy than that of the AA stacking structure and that the interlayer distance of the AB stacking is smaller than that of the AA stacking [73].

Next, we perform VDWDFT calculations to evaluate the interlayer distance of the graphite. We find that the interlayer distance of the AB stacking structure is 3.50 Å which is close to previously calculated result based on the VDWDFT (3.59 Å) [74]. Our result is somewhat larger than that of the experimental value (3.35 Å). This small overestimation seems to be reasonable because it was reported that the VDWDFT tends to overestimate the equilibrium distance [75]. The energy of the AB stacking structure is 3.80 meV/atom lower than that of the AA stacking structure (Table 3.1). As well as the LDA calculations, the VDWDFT calculations lead to the conclusion that the interlayer distance of the AA stacking structure (3.65 Å) is larger than that of the AB stacking structure (3.50 Å).

Here we carry out first principles calculations of the two-layer graphene. First we use the

Table 3.1: Calculated results of the graphite. d_{AB} (d_{AA}) represents the layer distance of the AB (AA) stacking. ΔE is the difference between the energies of the AB and AA stacking structures. ϵ_{AB} and ϵ_{AA} are the interlayer binding energies of the AB stacking and AA stacking structures, respectively.

	d_{AB} (Å)	d_{AA} (Å)	ΔE/atom (meV)	ϵ_{AB} (meV)	ϵ_{AA} (meV)
LDA	3.35 , 3.33 [a]	3.60	11.0	30.5	19.5
VDWDFT	3.50 , 3.59 [b]	3.65	3.80	31.0	27.2
Expt.	3.35 [c]				

[a] Ref. [72], [b] Ref. [74], and [c] Ref. [71].

LDA and find that the interlayer distance of the two-layer graphene of the AB stacking structure (3.35 Å) is the same as the corresponding value of the graphite. We also study the AA stacking structure and find that its energy is 6.0 meV/atom higher than that of the AB stacking structure. The calculated interlayer distance (3.60 Å) is larger than that of the AB stacking (3.35 Å) as shown in Table 3.2.

We next employ the VDWDFT in the calculation of the two-layer graphene. We find that interlayer distance of the AB stacking structure (3.49 Å) is close to than the corresponding value of the graphite (3.50 Å). We also study the AA stacking structure and find that its energy is 3.0 meV/atom higher than that of the AB stacking structure. As well as the LDA calculation, the VDWDFT calculation gives the result that the interlayer distance of the AA stacking (3.65 Å) is larger than that of the AB stacking (3.49 Å) as shown in Table 3.2.

We here study the interlayer binding energy (ϵ) of the AB stacking structure of graphite. The LDA and the VDWDFT give the energies of 30.5 and 31.0 meV/atom, respectively. Our value based on the LDA is comparable with those of the previous LDA calculations (20-30 meV/ atom) [76, 77, 78, 79]. The estimated values based on the LDA (30.5 meV/atom) and the VDWDFT (31.0 meV/atom) are close to previously experimental values (22-52 meV/atom)

Table 3.2: Calculated results of the two-layer graphene. d_{AB} (d_{AA}) represents the layer distance of the AB (AA) stacking. ΔE is the difference between the energies of the AB and AA stacking structures. ϵ_{AB} and ϵ_{AA} are the interlayer binding energies of the AB stacking and AA stacking structures, respectively.

	d_{AB} (Å)	d_{AA} (Å)	ΔE/atom (meV)	ϵ_{AB} (meV)	ϵ_{AA} (meV)
LDA	3.35	3.60	6.0	16.5	10.5
VDWDFT	3. 49	3.65	3.0	17.5	14.5

[80, 81] (Table 3.1) .

Next we study the interlayer binding energies of the two-layer graphene. The values based on the LDA and the VDWDFT are 16.5 meV/atom and 17.5 meV/atom, respectively (Table II). Therefore, we conclude that the interlayer binding energy of the two-layer graphene is smaller than that of graphite.

As mentioned above, our LDA and VDWDFT calculations show that the interlayer distance of the two-layer graphene having the AB stacking structure is very close to that of the graphite having the same stacking. On the other hand, a previous GGA calculation showed that the interlayer distance of the two layer graphene (3.58 Å) is larger than that of the graphite (3.26 Å) [67]. We perform GGA calculations by using the primitive cell and $18 \times 18 \times 1$ k-point mesh. These conditions are similar to those in the previous calculation [67]. We do not find stable structure; i.e. the two-layer graphene is not bound. In any case, the GGA is not suitable for calculations of van der Waals systems.

Based on the results of our LDA and VDWDFT calculations in this study, we conclude that the interlayer distance of the metastable AA stacking structure of the two-layer graphene is somewhat larger than that of the AB stacking structure. Therefore, it is suggested that the interlayer distance becomes large when the stacking deviates from the AB stacking. We also find that the interlayer distances of graphite and the two-layer graphene are very close. So, it

is suggested that the deviation from the AB stacking in two-layer graphitic systems leads to the layer distances which are larger than that of the graphite. This deviation from the AB stacking is expected to occur in the case of double wall and multiwall carbon nanotubues since the two nearest neighbor tubes have different radii.

3.2 Conclusion

In summary, we have carried out first principles DFT calculations using the LDA, GGA and the VDWDFT to investigate the interlayer distance of the two-layer graphene. We found that the interlayer distance is the same as that of the graphite. The binding energy of the graphite was found to be larger than that of the two-layer graphene. The interlayer distance of the metastable AA stacking structure of the two-layer graphene is larger than that of the AB stacking structure . It is thus suggested that the interlayer distance becomes somewhat large when the stacking is deviated from the AB stacking.

Chapter 4

Atomic hydrogen adsorption in graphenes and CNTs

In this chapter, we study atomic hydrogen adsorption in graphenes and CNTs. Under atomic hydrogen atmospheres, hydrogen atoms are chemisorbed on graphene and CNTs [24, 25, 26, 27, 28, 29, 30, 31, 32, 33, 34, 35, 36, 37, 38, 39, 40]. Scanning tunneling microscopy and photoluminescence spectroscopy showed that some hydrogen atoms are chemically adsorbed on carbon materials [36, 37, 38, 39, 40]. Then, first-principles calculations were performed for chemisorbed hydrogen [24, 25, 26, 27, 41, 42, 43]. As a result, it became clear that hydrogen significantly affects the physical properties of carbon nanomaterials. Hydrogen adsorption was found to affect the field emission of capped CNTs [44]. It was theoretically reported that some partially hydrogenated graphenes show ferromagnetic properties [45]. This result indicated that the magnetism of carbon nanomaterials can be controlled by hydrogen chemisorption.

To understand the effect of hydrogen adsorption, the study of monomers and dimers is necessary since they are fundamental hydrogen impurities in carbon materials.The electronic structure of hydrogen monomers in graphene has been well theoretically studied [24, 29, 48]. These theoretical studies showed that hydrogen is bonded to a host carbon atom and has a magnetic moment of 1 μ_B [24]. For dimers in graphene, the geometry where the two hydrogen atoms are on the same side has been studied [24, 25, 33, 34]. However, as mentioned later, we

find in this study that this geometry is metastable. Details of the electronic structures including the magnetism of the monomers and dimers in the CNTs are still unclear.

In this study, we perform first-principles calculations based on the spin-polarized generalized gradient approximation (GGA) [54] on graphene. It is expected that there will be some difference between graphene and CNTs because CNTs have curvature. To clarify the curvature effect, we study the armchair edge (5, 5) CNT and zigzag edge (10, 0) CNT, whose radii are 3.5 and 4.0 Å, respectively.

4.1 Graphene

4.1.1 GGA calculations

We first carry out spin-polarized GGA calculations of the monomer in graphene. The hydrogen atom is bonded to one of the carbon atoms on graphene plane and C-H bond length is 1.14 Å. This bond length is close to that in a CH_4 molecule (1.09 Å), which is typical sp^3 C-H bond lenghth. The distance between the graphene plane and the C atoms bonded to the hydrogen atoms is 0.37 Å. The bond lengths between the first and second nearest carbon atoms is 1.49 Å, which is larger than the graphene bond length (1.42 Å) and shorter than the diamond bond length (1.54 Å). The bond angle H-C1-C2 [Fig. 4.1] is 103.5 ° which is close to sp^3 bond angle (109.5°). The most stable geometry is found to be spin-polarized and has a magnetic moment of 1 μ_B. We show spin density distribution in Fig. 4.5(a). The binding energy Eq. (2.89) of the geometry is 0.53 eV. The information on the binding energy and magnetic moment is tabulated in Table 4.1.

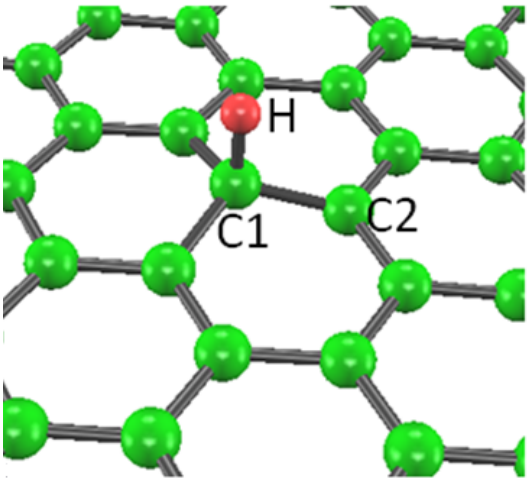

Figure 4.1: Geometrical configuration of the hydrogen monomer in graphene.

Next, we carry out calculations of the hydrogen dimer in graphene. In the most stable geometry of the dimer, both hydrogen atoms are bonded to carbon atoms which are nearest-neighbors. The two hydrogen atoms are located on opposite sides [Fig. 4.2(a)]. We find that the C1-C2 bond length [Fig. 4.2(a)] is 1.51 Å and the bond angle of H1-C1-C2 [Fig. 4.2(a)] is 107.8° . The bond length is close to the sp^3 bond length (1.54 Å) in diamond and the bond angle is close to the sp^3 bond angle (109.5°). In the most stable geometry of the dimer, the distance between the graphene plane and the C atoms bonded to the hydrogen atoms is 0.30 Å. This distortion of the carbon atoms is expected to be due to fact that the atoms have four surrounding atoms including the hydrogen atoms, and therefore the C atoms favor sp^3 hybridization. Since the sp^3 bond angle is less than 120°, the C atoms are displaced from the graphene plane. Previously the geometry where the two hydrogen atoms are located on the same side [Fig. 4.2)] was studied, [24] but we find that this geometry is metastable, i.e., its energy is 0.60 eV higher than that of the most stable geometry. The calculated bond angle of H1-C1-C2 [Fig. 4.2(b)] in the metastable geometry is 104.8°, which somewhat deviates from the sp^3 bond angle. As a result, the C1-C2 bond length (1.54 Å) is longer than that (1.51 Å) of the most stable geometry. Therefore, it is expected that the higher energy of the metastable geometry is due to the deviation from the sp^3 hybridization.

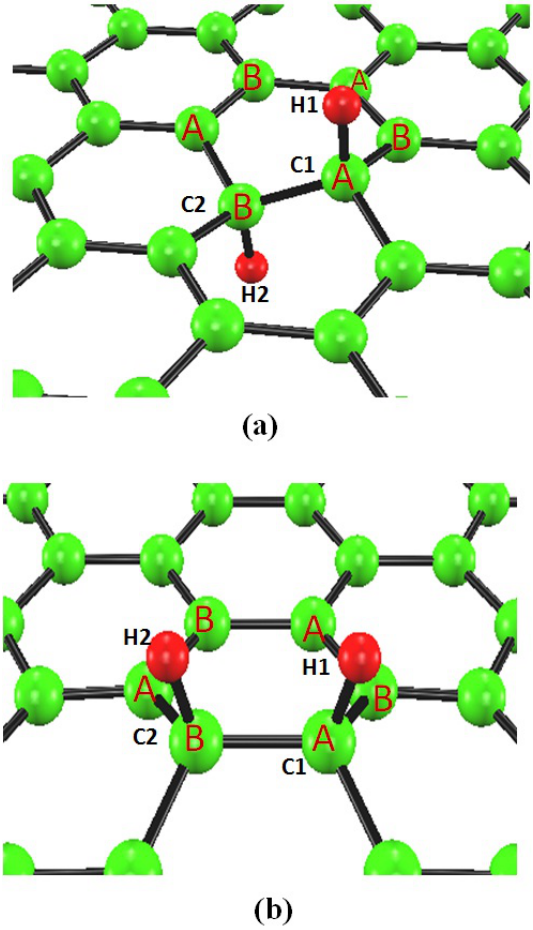

Figure 4.2: Nearest-neighbor geometrical configurations of the hydrogen dimers in graphene. A and B represent the A sublattice and B sublattice, respectively.

We show the charge densities of the most stable hydrogen dimer in Fig. 4.3(a) and those of the metastable hydrogen dimer in Fig. 4.2(b). In both dimers, we find a covalent bond charge between the hydrogen atom and its nearest carbon atom. These bonding charges are similar to that of the CH_4 molecule having the C-H sp^3 bond. The distances between the two hydrogen atoms are 3.07 Å [Fig. 4.3(a)] and 2.14 Å [Fig. 4.3(b)]. Since the distances are much larger than the bond length of the hydrogen molecule (0.74 Å), substantial charge density between the hydrogen atoms does not appear [Figs. 4.3(a) and 4.3(b)].

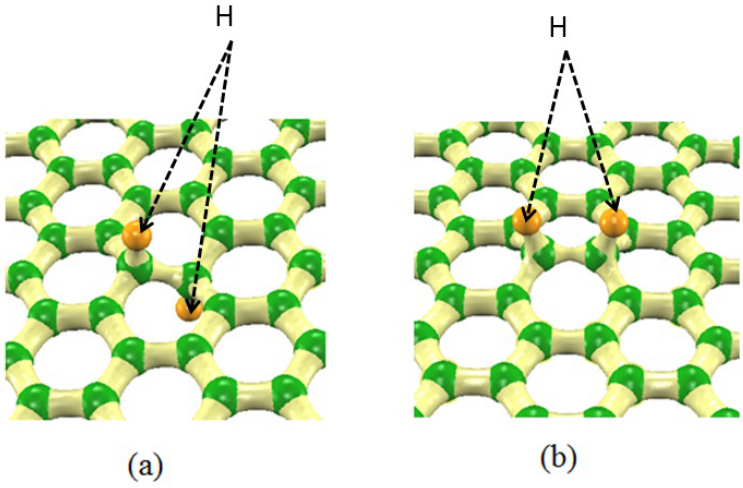

Figure 4.3: Charge densities of the hydrogen dimers where both of the hydrogen atoms are located on opposite sides (a) and on the same side (b) of graphene. The isosurface value is 0.22 $(a.u)^{-3}$.

The binding energy Eq. (2.89) per hydrogen atom of the most stable geometry of the dimer is calculated to be 1.16 eV. This value is much bigger than the binding energy of hydrogen monomer (0.53 eV). Therefore, the dimer is much more stable than the monomer. This stability of the dimer is roughly explained as follows on the basis of the bond-counting model, which has been used to analyze the stabilities of Si multivacancies and ultrathin Bi films [82, 83]. In the case of the monomer, the hydrogen atom is bonded to one of the carbon atoms, and three C-C bonds are strongly affected and weakened. The length of the C-C bond is 1.49 Å, which is longer than that of the pristine graphene (1.42 Å). Meanwhile, five C-C bonds are weakened in the case of the most stable dimer. Thus, the fact that the binding energy per atom of the dimer is higher than that of the monomer is expected to be due to the difference between the number of bonds weakened by the monomer and dimer, i.e., the number of weakened bonds per hydrogen atom is 3 for the isolated hydrogen monomer and 2.5 for the dimer.

Next, we study the case that the two hydrogen atoms are bonded to second-nearest-neighbor carbon atoms. The energy in the case that the two hydrogen atoms are located on opposite sides [Fig. 4.4(a)] is 0.10 eV lower than that when the two hydrogen atoms are on the same side [Fig.

4.4(b)] and 1.57 eV higher than that of the most stable geometry where the two hydrogen atoms are bonded to nearest-neighbor carbon atoms [Fig. 4.2(a)]. The bond angle of H2-C3-C2 in Fig. 4.4(a) is 104.0°, which is larger than that in Fig. 4.4(b) (102.4 °). Therefore, the former angle is closer to the sp^3 bond angle than the latter bond angle, which is expected to be the origin of the energetic stability of the former geometry.

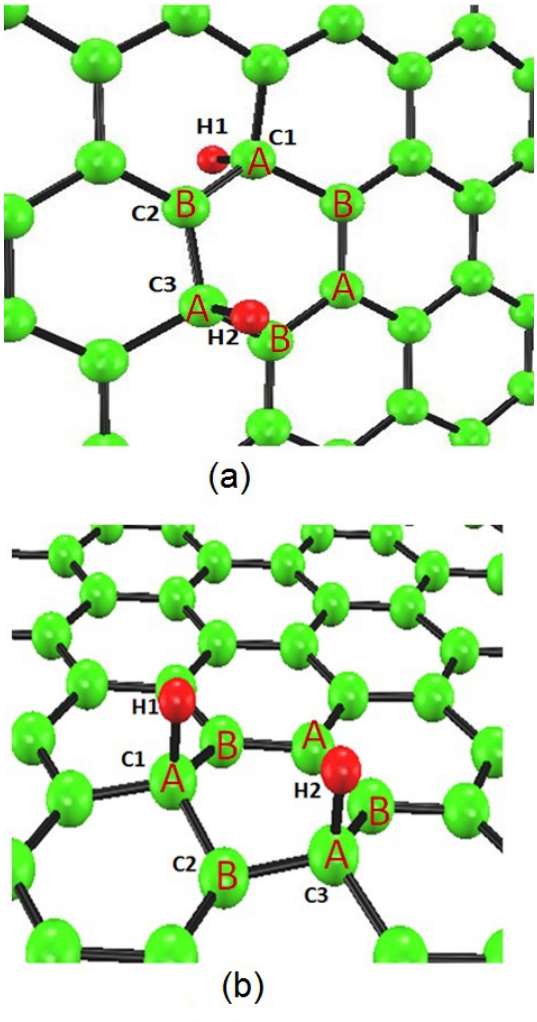

Figure 4.4: Second-nearest-neighbor geometrical configurations of the hydrogen dimers in graphene. A and B represent the A sublattice and B sublattice, respectively.

Both geometries are found to be spin-polarized and have magnetic moments of 2 μ_B. In the monomer case, one hydrogen provides one electron, which gives a magnetic moment of 1 μ_B.

However, in the case of the hydrogen dimer, the two hydrogen atoms provide two electrons. Therefore, when magnetization is realized, the magnetic moment is 2 μ_B. The nonmagnetic state of the geometry in Fig. 4.4(a) has 0.13 eV higher energy than that of the spin-polarized state. As shown in Fig. 4.5(b), a large spin density is located at the hydrogen site and the graphene sublattice, which is different from the sublattice to which the hydrogen is bonded. This result indicated that the hydrogen s-orbital is hybridized with the wavefunction at the Dirac cone point of graphene. The wavefunction having a nonzero amplitude at only one sublattice originates from those of the Dirac points. Similar hybridization occurs for the hydrogen monomer in graphene [Fig. 4.5(a)]. This spin distribution of the monomer was also previously reported [24, 48] and explained on the basis of spin alternation [42]. Similar spin density of the monomer was also found for the CNTs as discussed in sect. 4.2 and sect. 4.3. The reason for the magnetization will be discussed in sect. 4.3 on the basis of the calculated density of states (DOS).

We found that when the two hydrogen atoms are bonded to third-nearest-neighbor carbon atoms, the electronic structure is nonmagnetic. In the nearest-neighbor and third-nearest-neighbor configurations, the two hydrogen atoms are bonded to different sublattices, i.e., the A and B sublattices. In this case, no spin polarization arises and magnetization is not achieved. On the other hand, when the two hydrogen atoms are bonded to the second-nearest-neighbor carbon atoms, both hydrogen atoms are bonded to the same (A) sublattice and the majority spin density appears at the B sublattices.

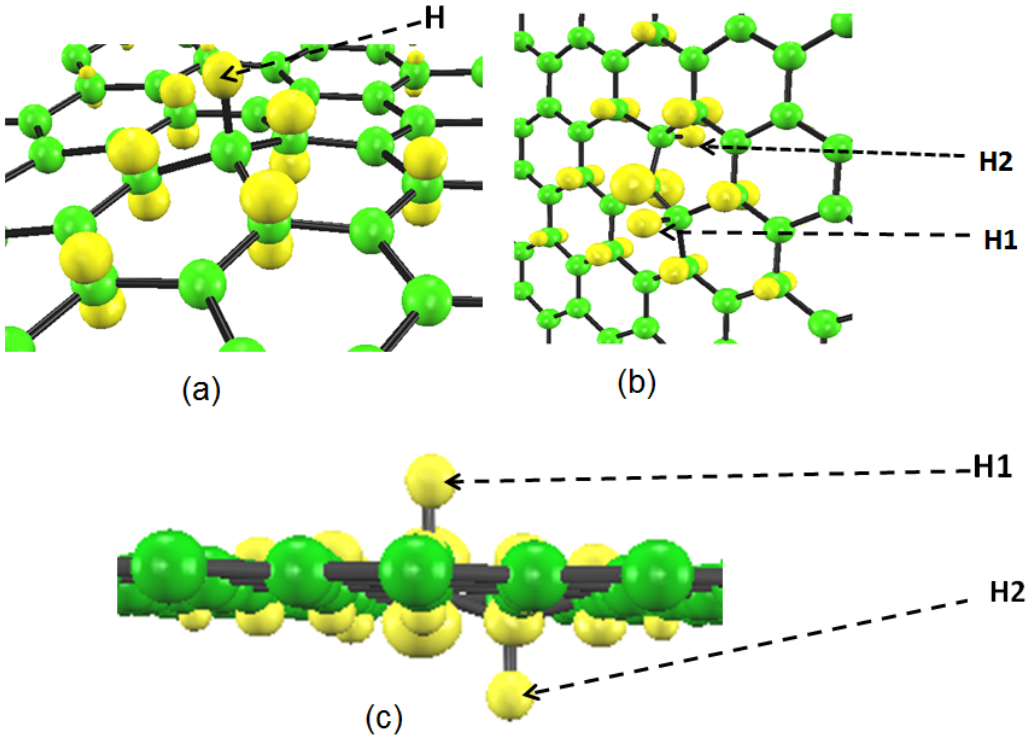

Figure 4.5: Spin density distributions of the hydrogen monomer (a) and hydrogen dimer (b, c) having second-nearest-neighbor geometry [Fig. 4.4(a)] in graphene. The isosurface value is 0.01 $(a.u)^{-3}$.

4.1.2 LDA calculations

Here we use the local spin density approximation (LSDA) treatment for exchange and correlation as it more accurately describes the weak molecular H_2-carbon interaction [84, 85]. We first perform calculations of mono hydrogen on graphene. The hydrogen atom is bonded to one of the carbon atoms on graphene plane and C-H bond length is 1.14 Å. This bond length is close to that in a CH_4 molecule (1.09 Å), which is typical sp^3 C-H bond lenghth. The distance between the graphene plane and the C atoms bonded to the hydrogen atoms is 0.33 Å. The bond lengths between the first and second nearest carbon atoms is 1.49 Å, which is larger than the graphene bond length (1.42 Å) and shorter than the diamond bond length (1.54 Å). The bond

angle H-C1-C2[Fig. 4.6] is 102.3° which is close to sp^3 bond angle (109.5°). The most stable geometry is found to be spin-polarized and has a magnetic moment of 1 μ_B. The spin density is located at hydrogen site and graphene subattices where the hydrogen atom is bonded. This spin distribution is similar to that of GGA calculation in grahene [Fig. 4.5(a)].The binding energy of the geometry is 1.11 eV [Table 4.2]. We note that our calculated value is comparable with a previous calculation based on the LDA (1.32 eV) [35]. This binding energy is larger that of GGA calculation (0.53eV) as LDA overestimates the binding energy.

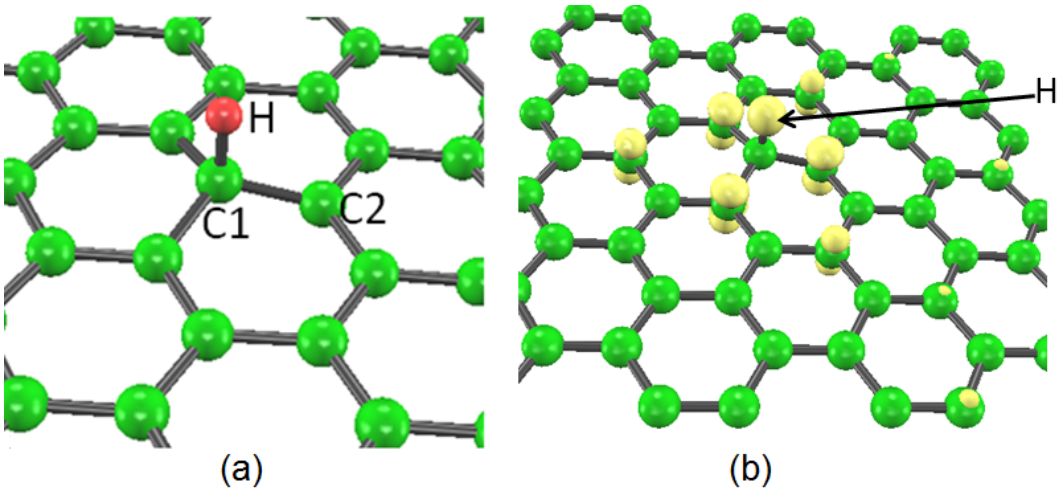

Figure 4.6: Geometrical configuration of the hydrogen monomer (a) and spin density distribution (b) in the graphene. The isosurface value is 0.01 $(a.u)^{-3}$.

Next, we carry out calculations of the hydrogen dimer in graphene. In the most stable geometry of the dimer, both hydrogen atoms are bonded to carbon atoms which are nearest-neighbors. The two hydrogen atoms are located on opposite sides [Fig. 4.7(a)]. We find that the C1-C2 bond length [Fig. 4.7(a)] is 1.51 Åand the bond angle of H1-C1-C2 [Fig. 4.7(a)] is 106.3°. The bond length is close to the sp^3 bond length (1.54 Å) in diamond and the bond angle is close to the sp^3 bond angle (109.5°). We find that the geometry where the two hydrogen atoms are located on the same side [Fig. 4.7)(b)] has 0.65 eV higher energy than that of the most stable geometry. This energy difference is close to (0.60 eV) that of GGA calculations as described in sect. 4.1. The calculated bond angle of H1-C1-C2 [Fig. 4.7(b)] in the metastable

geometry is 104.1°, which somewhat deviates from the sp^3 bond angle. As a result, the C1-C2 bond length (1.54 Å) is longer than that (1.51 Å) of the most stable geometry. Therefore, it is expected that the higher energy of the metastable geometry is due to the deviation from the sp^3 hybridization.

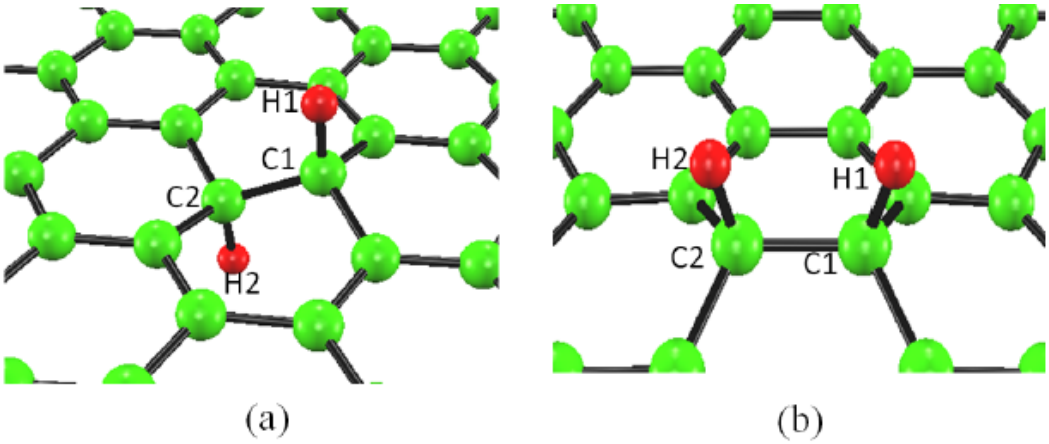

Figure 4.7: Geometrical configuration of the hydrogen dimer in graphene

The binding energy per hydrogen atom (E_b) Eq. (2.89) of the most stable geometry of the dimer is calculated to be 1.95 eV [Table 4.2]. We calculate the binding energy (E_b) of monomer to be 1.14 eV. This value is much smaller than the binding energy per hydrogen atom of the most stable geometry of the dimer (1.95 eV). Thus, the dimer is much more stable than the monomer. The same result also found for GGA calculations in sect. 4.1.

Next, we study the case that the two hydrogen atoms are bonded to second-nearest-neighbor carbon atoms. The energy in the case that the two hydrogen atoms are located on opposite sides [Fig. 4.8(a)] is 0.10 eV lower than that when the two hydrogen atoms are on the same side [Fig. 4.8(b)] and 1.70 eV higher than that of the most stable geometry where the two hydrogen atoms are bonded to nearest-neighbor carbon atoms [Fig. 4.7(a)]. This energy difference is close to that of GGA calculations 1.57 eV sect. 4.1. The bond angle of H2-C3-C2 in Fig. 4.8(a) is 102.3°, which is larger than that in Fig. 4.8(b) (101.8°). Therefore, the former angle is closer to the sp^3 bond angle than the latter bond angle, which is expected to be the origin of the energetic stability of the former geometry.

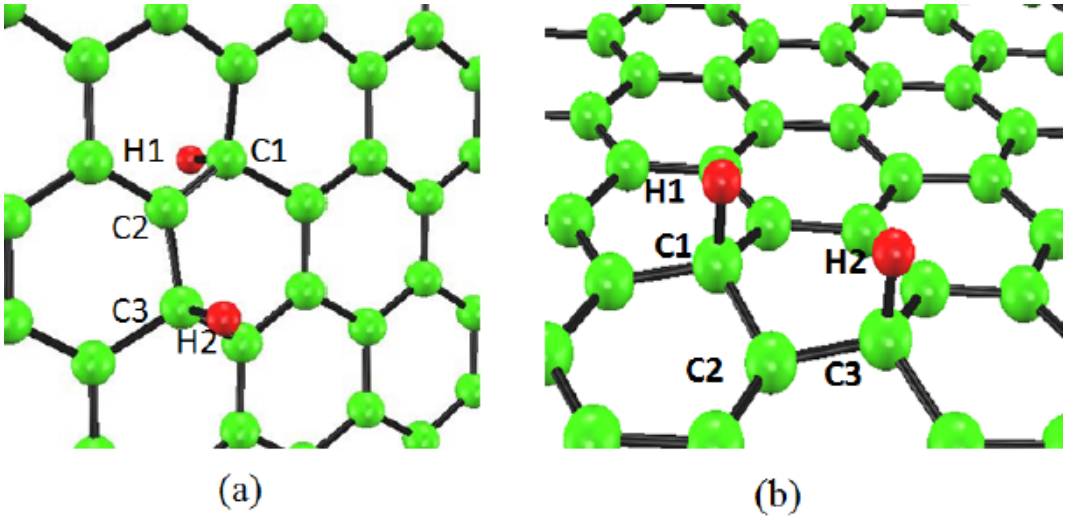

Figure 4.8: Second-nearest-neighbor geometrical configuration of the hydrogen dimer in graphene.

Both geometries are found to be spin-polarized and have magnetic moments of 2 μ_B. In the monomer case, one hydrogen provides one electron, which gives a magnetic moment of 1 μ_B. However, in the case of the hydrogen dimer, the two hydrogen atoms provide two electrons. Therefore, when magnetization is realized, the magnetic moment is 2 μ_B. We show the spin density distribution in Fig. 4.9 and we find that the spin density distribution is same as shown in Fig. 4.5(b), a large spin density is located at the hydrogen site and the graphene sublattice, which is different from the sublattice to which the hydrogen is bonded.

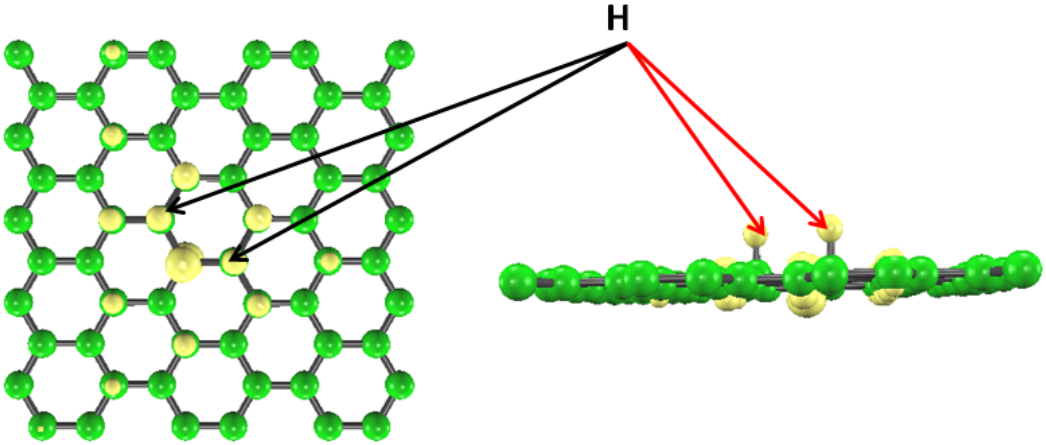

Figure 4.9: Spin density distribution of the hydrogen dimer having second-nearest-neighbor geometry [Fig. 4.8(b)] in the mono-layer graphene. The isosurface value is 0.01 $(a.u)^{-3}$.

As mentioned above in sections 4.1.1 and 4.1.2, we find that binding energies of hydrogen monomer calculated by GGA and LDA are 0.53 eV and 1.11 eV, respectively. This overestimation seems to be reasonable because it was reported that the binding energies are typically overestimated, sometimes even by a factor of two [86] in LDA. Calculations perform by GGA and LDA show that monomers are spin-polarized and have magnetic moment 1 μ_B. The binding energies per hydrogen atom of the most stable dimers calculated by GGA and LDA are 1.16 eV and 1.95 eV, respectively and their electrons structures are nonmagnetic. However, in LDA we find that the geometry where the two hydrogen atoms are located on the same side [Fig. 4.7(b)] has 0.65 eV higher energy than that of the most stable geometry [Fig. 4.7(a)]. This energy difference is close to (0.60 eV) that of GGA calculations as described in sect. 4.1. Both GGA and LDA show that second-nearest-neighbor geometries are spin-polarized and have magnetic moment 2 μ_B.

4.2 Armchair edge (5, 5) carbon nanotube

We perform spin-polarized GGA calculations of the monomers and dimers in armchair edge (5, 5) CNT. Before we study the dimer, the monomer is first investigated. In the most stable

geometry, the hydrogen atom is located on the outer side of the armchair edge (5,5) CNT and the atom is bonded to one carbon atom [Fig. 4.10(a)]. The geometry where the hydrogen atom is located inside the CNT [Fig. 4.10(b)] has a negative binding energy (Table 4.1). The bond angle of H1-C1-C3 [Fig. 4.10(a)] in the most stable geometry is 106.9° and that [Fig. 4.10(b)] in the metastable geometry is 98.8°. Therefore, the bond angle in the most stable geometry is close to the sp^3 bond angle. The bond length between the hydrogen atom and nearest-neighbor carbon atom is 1.12 Å for the most stable structure and is close to that of the CH_4 molecule (1.09 Å). The most stable geometry is found to be spin-polarized and has a magnetic moment of 1 μ_B. As shown in Fig. 4.10(c), the spin density is located at the hydrogen site and at the nearest and third-nearest-neighbors of the carbon atom where the hydrogen is bonded. This spin distribution is similar to that of graphene [Fig. 4.5(a)].

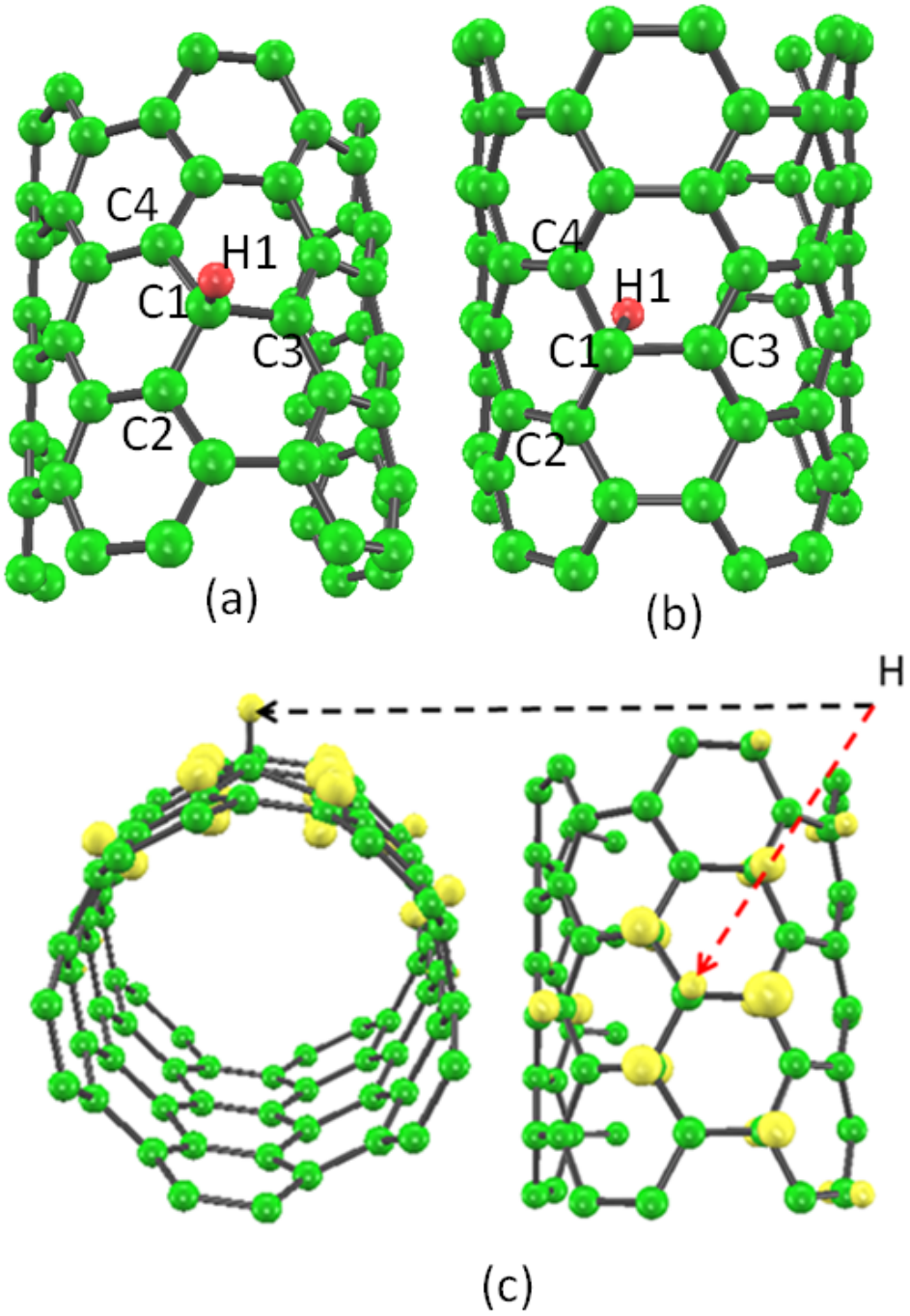

Figure 4.10: Geometrical configurations of the hydrogen monomer in the armchair edge (5,5) CNT [(a) and (b)], and spin density distributions of the former hydrogen monomer (c). The isosurface value is 0.01 $(a.u)^{-3}$.

The binding energy of the most stable geometry is calculated to be 1.13 eV [Table 4.1],

which is much larger than that of the hydrogen monomer in graphene (0.53 eV). This result implies that the CNT is easily hydrogenated compared with graphene. The bond lengths of the pristine CNT are 1.44 and 1.45 Å [Fig. 4.11(a)], which are larger than that of graphene (1.42 Å). Therefore, the rather weak bonds in the pristine CNT are expected to contribute to its large binding energy. Furthermore, the average bond angles of H-C-C in the armchair edge (5,5) CNT and graphene are 106.6 and 103.5°, respectively. Thus, the bond angle in the CNT is energetically favored since it is close to the sp^3 bond angle.

Now we study the dimer in the armchair edge (5,5) CNT. It is found to be energetically preferable that the two hydrogen atoms are on the outer side of the CNT. This is in contrast to the case of graphene, where the two hydrogen atoms are located on the different sides. The difference between graphene and the CNT is expected to originate from the fact that the CNT has curvature. As was discussed for the monomer case of the CNT, the hydrogen-carbon bond abgles are close to the sp^3 bond angle when the hydrogen atoms are located on the outer side, whereas the bond angles are small when the hydrogen atoms are located on the inner side. There are two types of geometry where both hydrogen atoms are on the outer side and are bonded to nearest-neighbor carbon atoms. In one geometry, the alignment of the two carbon atoms bonded to hydrogen atoms is in the tube direction [Fig. 4.11(c)], and in the other geometry, the alignment is tilted from the tube direction [Fig. 4.11(b)]. I find that the geometry in Fig. 4.11(b) has 0.20 eV lower energy than that in Fig. 4.11(c). The lengths of the C-C bonds in the pristine CNT are 1.44 and 1.45 Å in the cases of the tube direction and tilted direction, respectively. Therefore, the latter C-C bond is weaker than the former bond. This weakness is expected to be the origin of the energetic stability of the most stable geometry. The binding energy of the most stable geometry is 1.65 eV, which is much larger than that in graphene (1.16 eV).

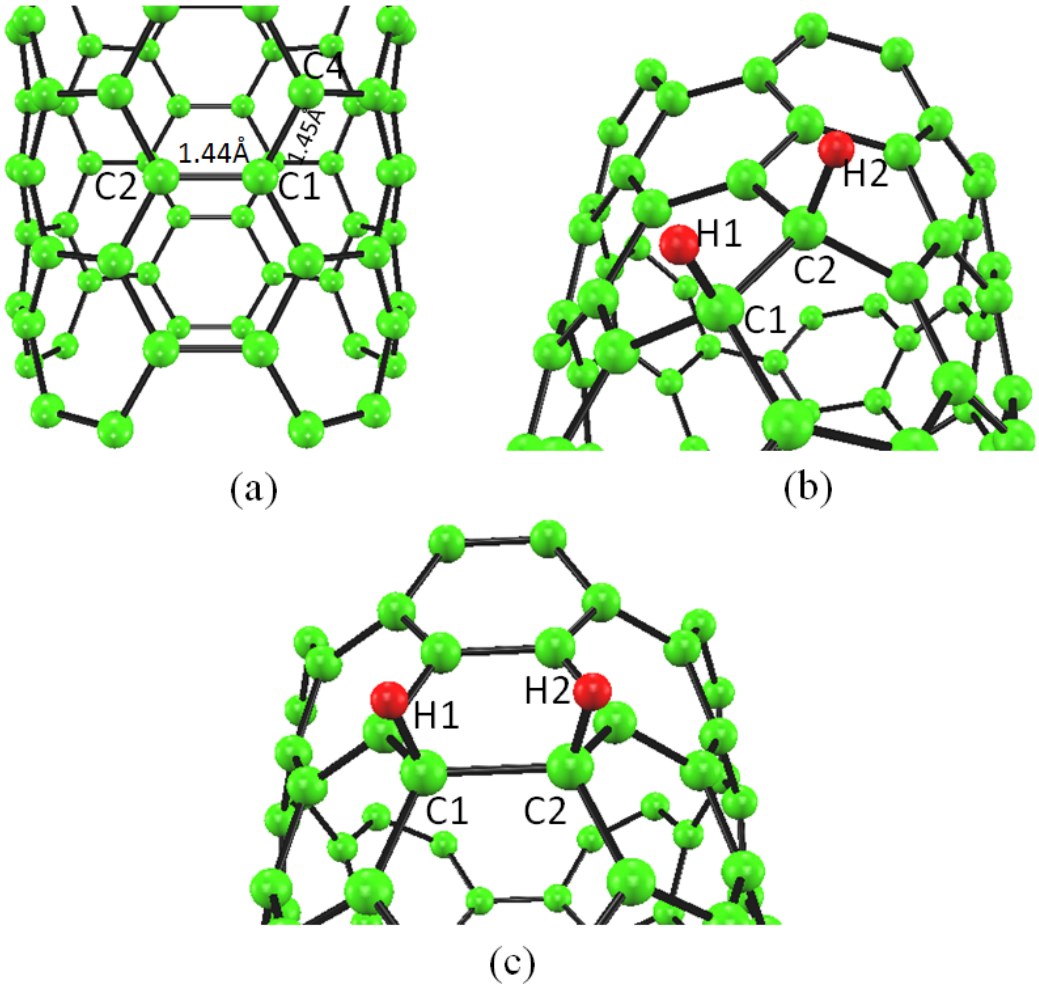

Figure 4.11: Geometrical configurations of the pristine armchair edge (5,5) CNT (a) and the hydrogen dimer in the armchair edge (5,5) CNT (b) and (c).

Next we study the case that the two hydrogen atoms are bonded to second-nearest-neighbor carbon atoms. We find that the bond angle of H1-C1-C2 [Fig.4.12(a)] is 108.3° and this geometry has 0.87 eV higher energy than that of the most stable structure. The geometry is found to be spin-polarized and has a magnetic moment of 2 μ_B. The nonmagnetic state has 0.21 eV higher energy than that of the spin-polarized state. As shown in Fig. 4.12(b1, b2), large spin densities appear at the hydrogen site and CNT sublattices, which are different from the sublattices, where the two hydrogen atoms are bonded.

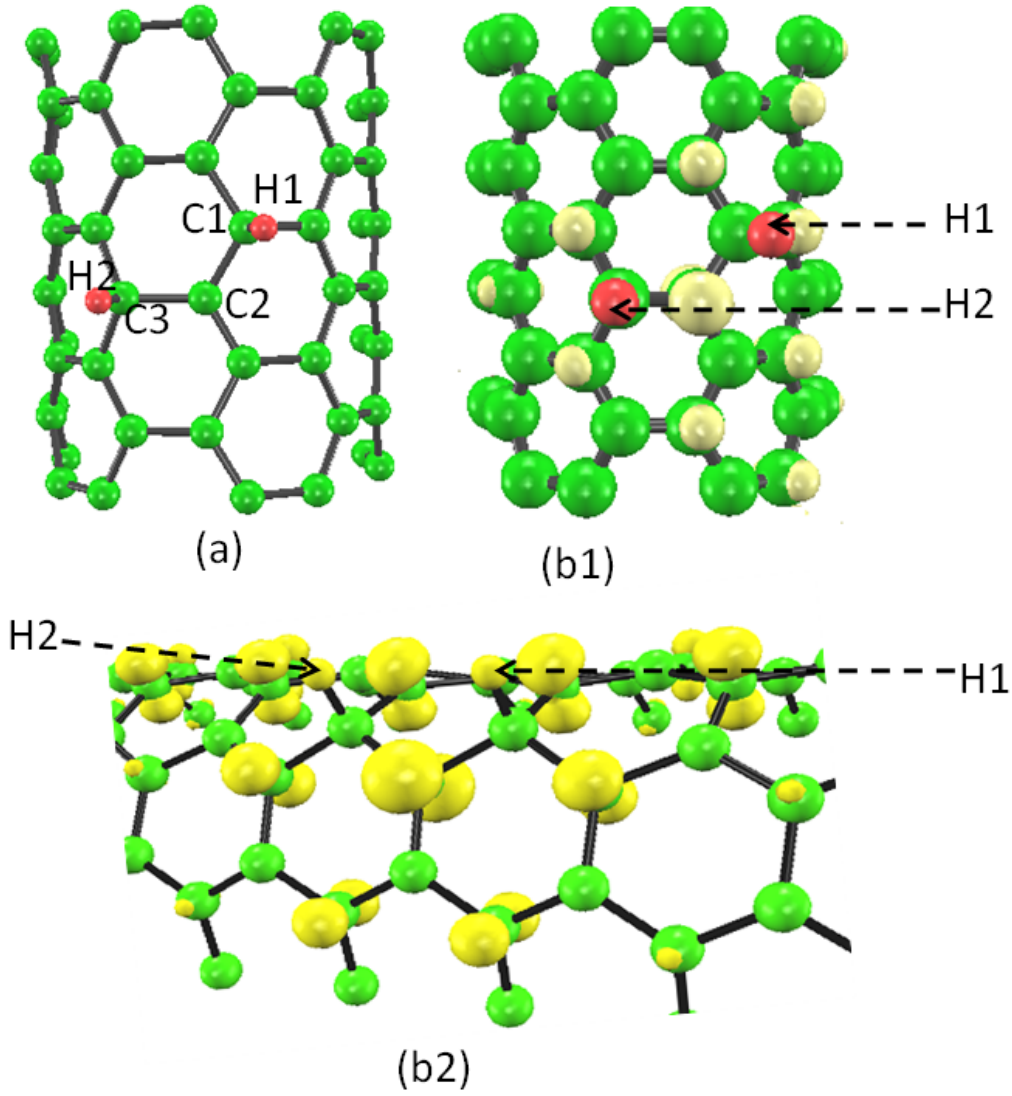

Figure 4.12: Geometrical configurations of the hydrogen dimer in the armchair edge (5,5) CNT having the second-nearest-neighbor (a) and spin density distributions of the hydrogen dimer (b1, b2). The isosurface value is 0.01 $(a.u)^{-3}$.

4.3 Zigzag edge (10, 0) carbon nanotube

Here we carry out spin-polarized GGA calculations of the monomers and dimers in zigzag edge (10, 0) CNT. In the most stable structure of the monomer, the hydrogen atom is located outside

the zigzag edge (10,0) CNT and the atom is bonded to one carbon atom [Fig. 4.13(a)]. This geometry is similar to that of the armchair edge (5,5) CNT. The geometry where the hydrogen atom is located inside the CNT [Fig. 4.13(b)] has 0.93 eV higher energy than that of the most stable geometry [Fig. 4.13(a)]. In the most stable geometry [Fig. 4.13(a)], the bond angle of H1-C1-C3 is 106.9° compare with 94.4° in the metastable structure [Fig. 4.13(b)]. Therefore, the bond angle in the most stable geometry is close to the sp^3 bond angle, which is expected to be the origin of the energetic stability. The bond length between the hydrogen atom and nearest-neighbor carbon atom is 1.12 Å which is the same as that in the armchair edge (5,5) CNT. The most stable and metastable geometries are found to be spin-polarized and have a magnetic moment of 1 μ_B. As shown in Fig. 4.13(c), the spin density is located at the hydrogen site and at the nearest and third-nearest-neighbors of the carbon atom where the hydrogen is bonded. This spin distribution is similar to that of the armchair edge (5,5) CNT [Fig. 4.12(b1, b2)] and graphene [Fig. 4.5(a)].

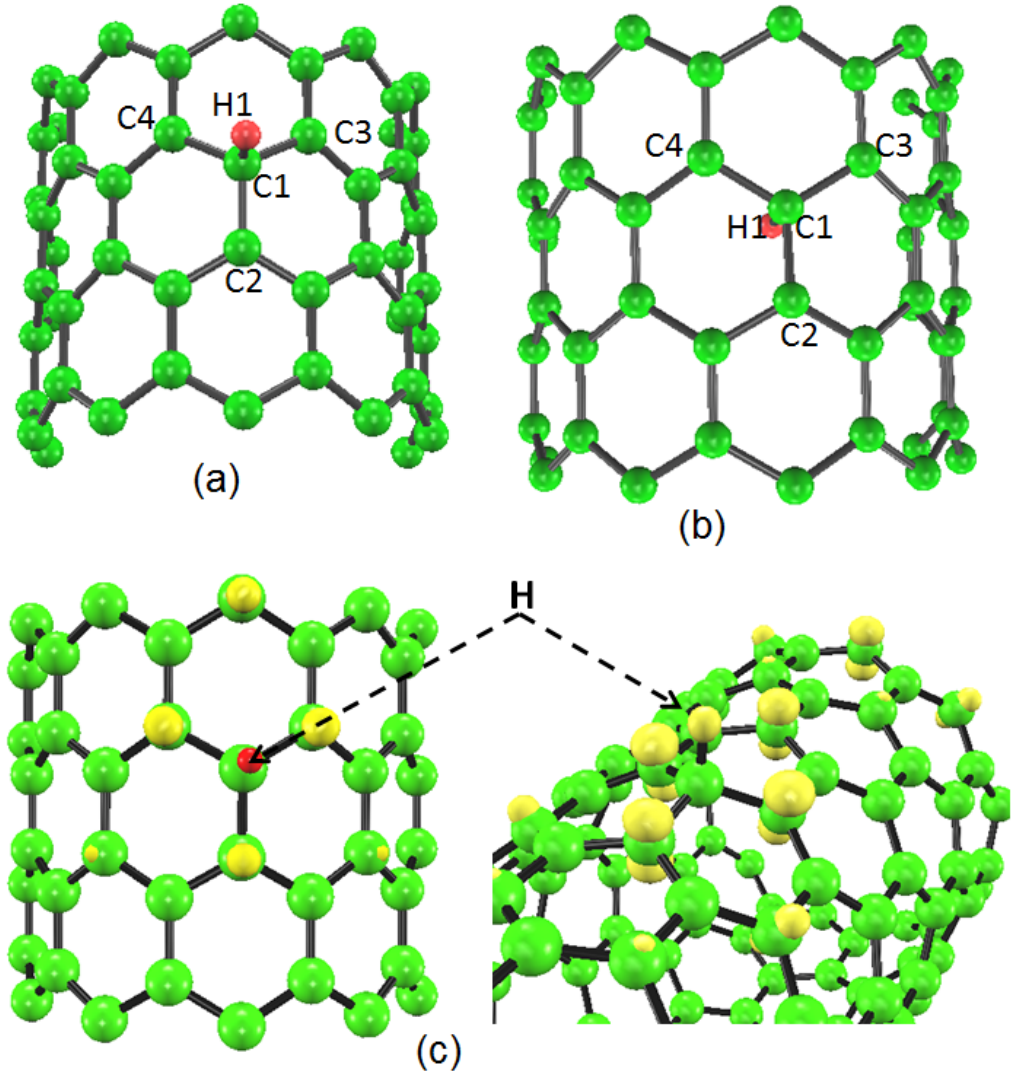

Figure 4.13: Geometrical configurations of the hydrogen monomer in the zigzag edge (10,0) CNT [(a) and (b)] and spin density distributions of the former hydrogen monomer (c). The isosurface value is 0.01 $(a.u)^{-3}$.

We show the DOS of the nonmagnetic state in Fig. 4.14(a). The sharp peak appears at the Fermi energy and the corresponding band is half occupied. In the case of spin polarization [Fig. 4.14(b)], the peak in the nonmagnetic state splits into two, and only the majority spin band is fully occupied. This split is expected to stabilize the spin-polarized state. Similar splits have also been confirmed for graphene[48] and the armchair edge (5,5) CNT. Therefore, we expect that the mechanisms of spin polarization are similar for graphene, the armchair edge (5,5) CNT,

and the zigzag edge (10,0) CNT. Note that the spin densities of graphene and the armchair edge (5,5) CNT are shown in Fig. 4.5(a) and Fig. 4.10(c), respectively.

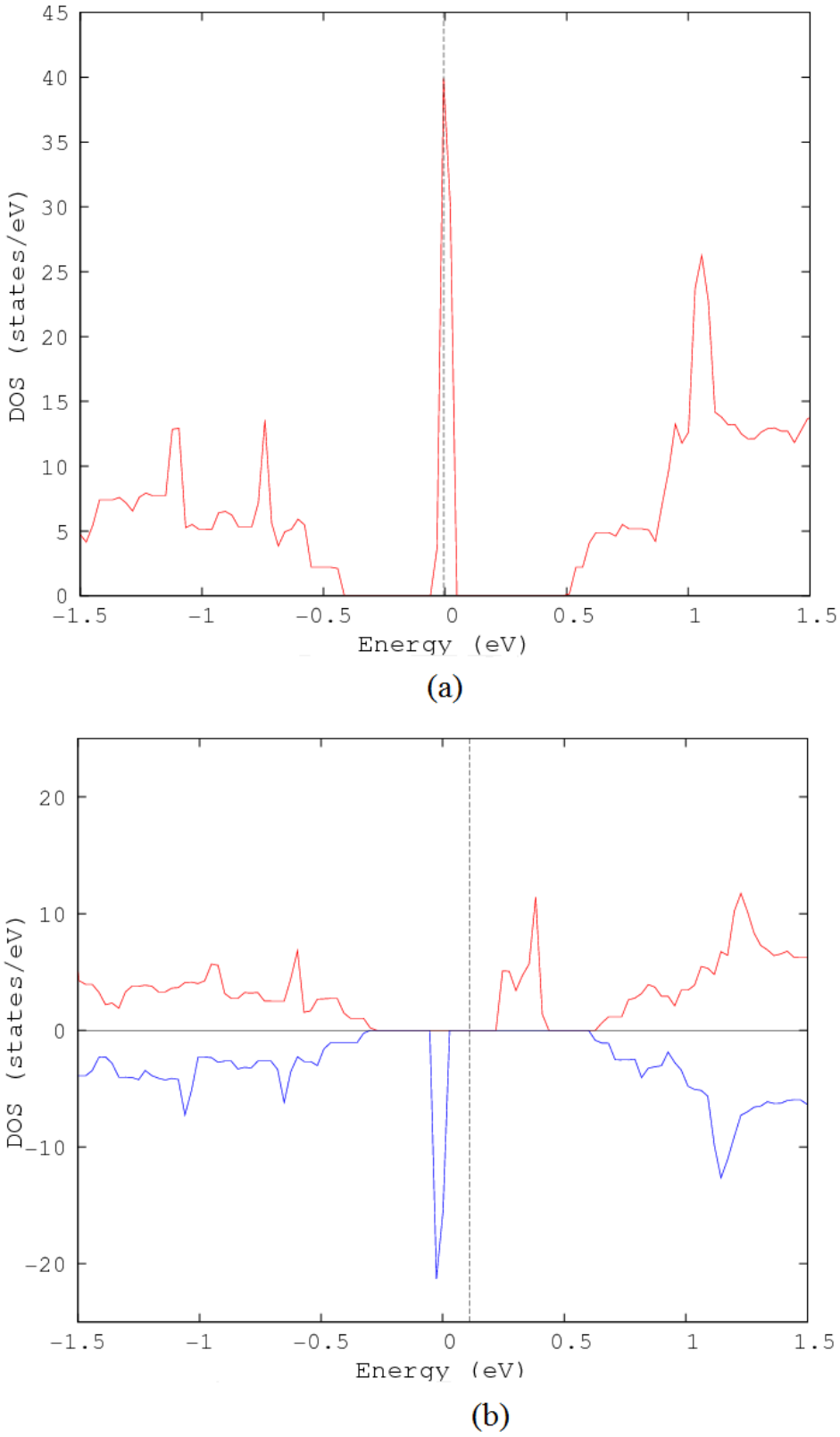

Figure 4.14: Density of states of the nonmagnetic electronic structure (a) and spin-polarized electronic structure (b) of the hydrogen monomer on the zigzag edge (10,0) CNT. The energies are measured from the Fermi energy. The lower and upper lines represent the majority and minority spins, respectively.

The binding energy of the most stable geometry is calculated to be 1.10 eV, which is much larger than that of the hydrogen monomer in graphene (0.53 eV) and close to the binding energy of the armchair edge (5,5) CNT (1.13 eV) (Table 4.1).

Table 4.1: Hydrogen monomers and dimers in graphene, armchair edge (5,5) CNT, and zigzag edge (10,0) CNT. NN and SN denote the nearest-neighbor and second-nearest-neighbor configurations, respectively.

	Position	Geometry Figure number	C-H bond length (Å)	Avg. H-C-C bond angle (°)	E_b eV	Magnetic moment μ_B
Graphene	Monomer	4.1	1.14	103.5	0.53	1
	NN dimers	4.2(a)	1.13	107.8	1.16	0
		4.2(b)	1.12	104.8	0.86	0
	SN dimers	4.4(a)	1.14	104.0	0.38	2
		4.4(b)	1.15	102.4	0.33	2
Armchair edge (5,5) CNT	Monomer	4.10(a)	1.12	106.6	1.13	1
		4.10(b)	1.14	98.8	-0.06	1
	NN dimers	4.11(b)	1.11	105.4	1.65	0
		4.11(c)	1.11	102.4	1.54	0
	SN dimers	4.12(a)	1.12	108.3	1.21	2
Zigzag edge (10,0) CNT	Monomer	4.13(a)	1.12	106.9	1.10	1
		4.13(b)	1.15	94.4	0.17	1
	NN dimers	4.15(b)	1.11	105.9	1.60	0
		15(c)	1.11	103.5	1.55	0
	SN dimers	4.16(a)	1.12	106.9	1.09	2

Next we carry out calculations for the dimer in the zigzag edge (10,0) CNT. It is found to be energetically preferable that the two hydrogen atoms are on the outer side of the CNT. There are two types of geometry where the two hydrogen atoms are located on the outer side and are bonded to nearest-neighbor carbon atoms. In one geometry, the alignment of the two carbon atoms bonded to hydrogen atoms is in the tube direction [Fig. 4.15(b)] and in the other geometry the alignment is tilted from the tube direction [Fig. 4.15)]. We find that the geometry in Fig. 4.15(b) has 0.07 eV lower energy than that in Fig. 4.15(c). The lengths of the C-C bonds in the pristine CNT are 1.45 and 1.44 Å in the cases of the tube direction and tilted direction, respectively. Therefore, the former bond is weaker than the latter bond, which is expected to be the origin of the most stable geometry. The binding energy of the most stable geometry is 1.60 eV, which is close to that of the armchair edge (5,5) CNT (1.65 eV) and much larger than that (1.16 eV) of graphene (Table 4.1).

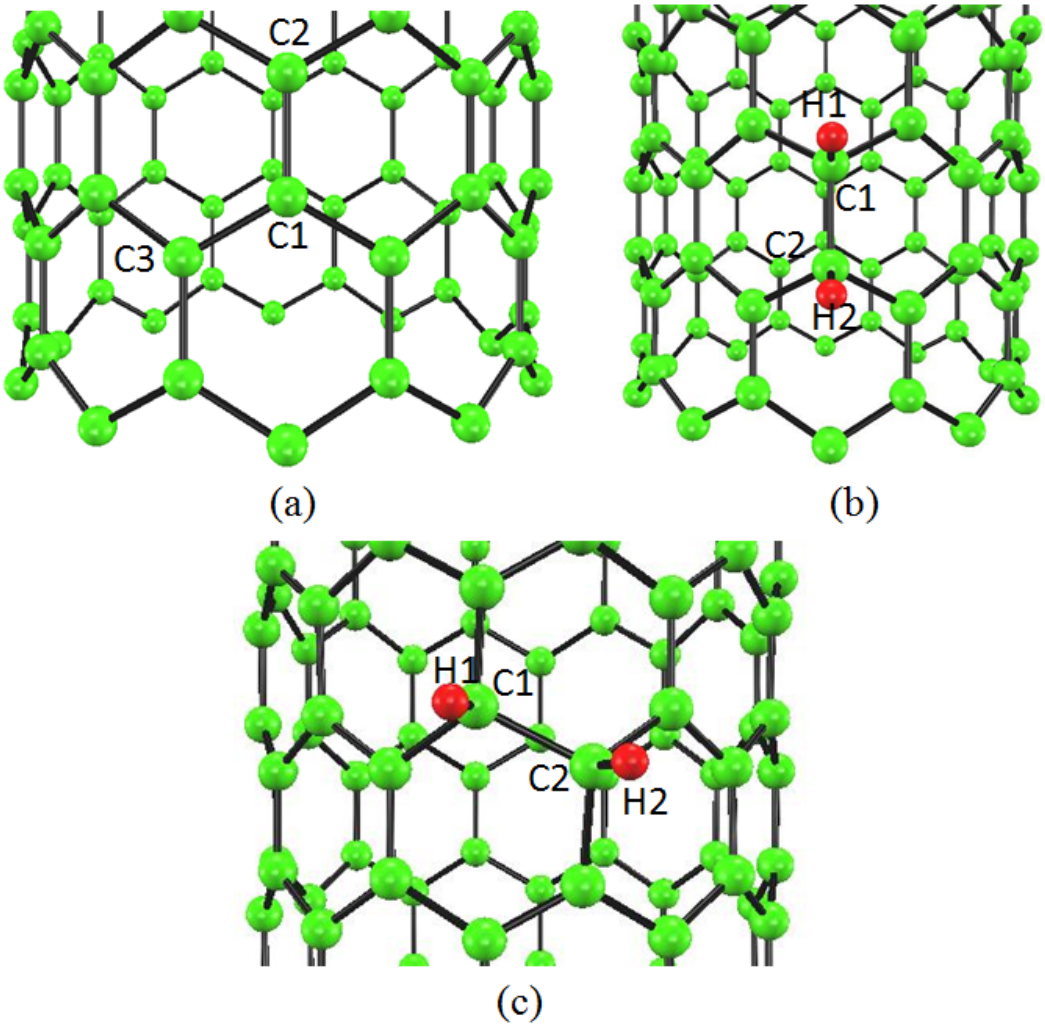

Figure 4.15: Geometrical configurations of the pristine zigzag edge (10,0) CNT (a) and the hydrogen dimer in the zigzag edge (10,0) CNT (b) and (c).

Finally we study the case that the two hydrogen atoms are bonded to second-nearest-neighbor carbon atoms. I find that the bond angle of H1-C1-C2 in Fig.4.16(a) is 106.9° and this geometry has 1.0 eV higher energy than that of the most stable structure. The geometry is found to be spin-polarized and has a magnetic moment of 2 μ_B. The energy gained by spin polarization is 0.11 eV. As shown in Fig. 4.16(b), large spin densities appear at the hydrogen site and CNT sublattice, which are different from the sublattice where the two hydrogen atoms are bonded. Therefore, this spin distribution is similar to those of the armchair edge (5,5) CNT [Fig. 4.12(b)]

and graphene [Fig. 4.5(b)].

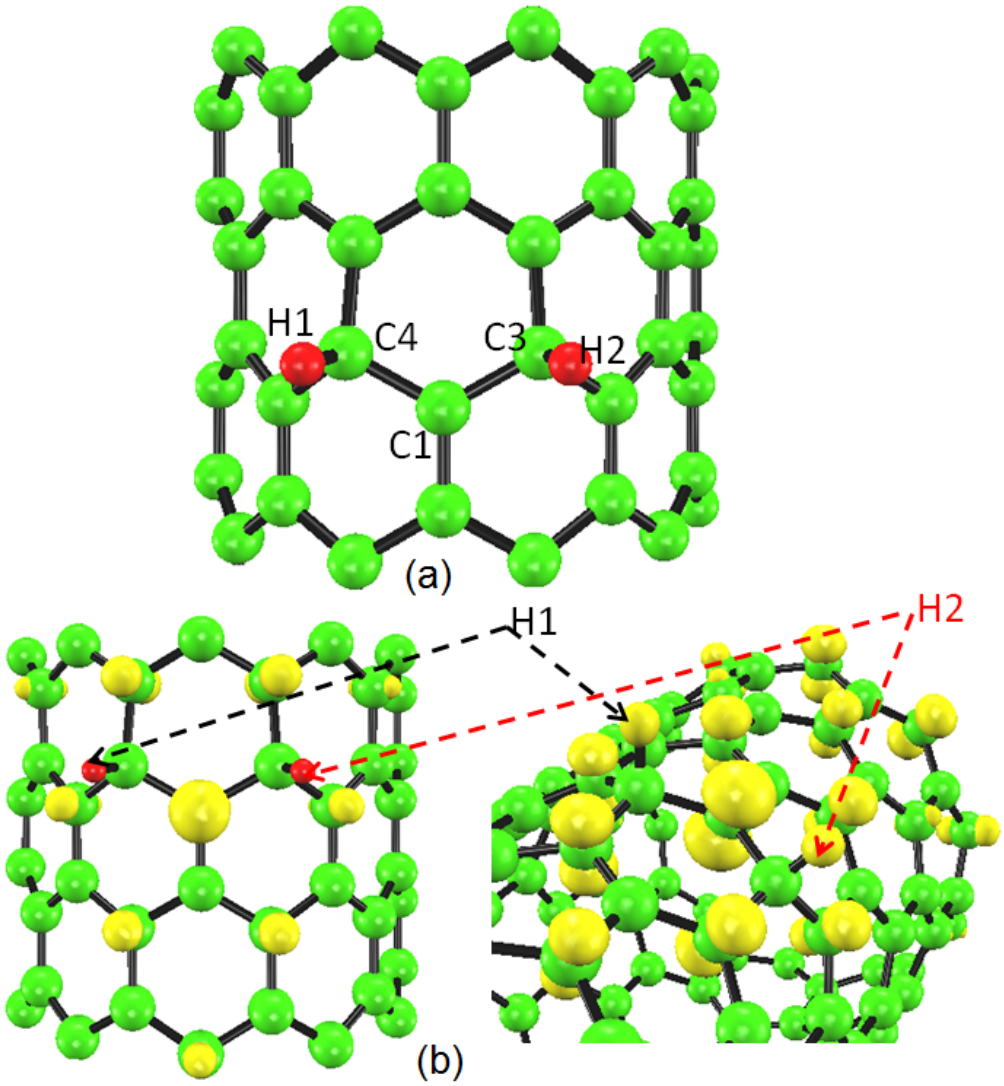

Figure 4.16: Second-nearest-neighbor geometrical configurations of the hydrogen dimer in the zigzag edge (10,0) CNT (a), and spin density distributions of the hydrogen dimer (b). The isosurface value is 0.01 $(a.u)^{-3}$.

Table 4.2: Hydrogen monomers and dimers in graphene. NN and SN denote the nearest-neighbor and second-nearest-neighbor configurations, respectively. E_b is the binding energy per hydrogen atom. These results are based on the LSDA calculations.

	Position	Geometry Figure number	C-H bond length (Å)	Avg. H-C-C bond angle (°)	E_b eV	Magnetic moment μ_B
Graphene	Monomer	4.6(a)	1.14	102.3	1.14	1
	NN dimers	4.7(a)	1.13	106.3	1.95	0
		4.7(b)	1.12	104.05	1.62	0
	SN dimers	4.8(a)	1.15	102.3	1.10	2
		4.8(b)	1.15	101.8	1.05	2

4.4 Conclusions

By using first-principles calculations based on the spin-polarized GGA within the density functional theory method, we studied hydrogen monomers and dimers in graphene, the armchair edge (5,5) CNT, and the zigzag edge (10,0) CNT. We found that the monomers are spin-polarized. The binding energies in the CNTs (1.13 and 1.10 eV) are found to be much larger than that of graphene (0.53 eV). Therefore, the CNTs are easily hydrogenated compared with graphene. In the most stable structures of the dimers in graphene and the CNTs, the two hydrogen atoms are bonded to the host carbon atoms which are nearest-neighbors. In the case of graphene, the two atoms are located on opposite sides. In contrast, in the cases of the armchair edge (5,5) CNT and zigzag edge (10,0) CNT, both hydrogen atoms are located on the outer side. When the two hydrogen atoms are bonded to the same sublattice of the host materials, magnetic moments of 2 μ_B appear in graphene and the CNTs.

We also carried out LSDA calculations of hydrogen monomer and dimers in graphene. We found that binding energies of monomer and most stable dimer calculated by LDA (GGA) are

1.11 (0.53) eV and 1.95 (1.16) eV, respectively. These overestimation are reasonable as LDA overestimates the binding energies. However magnetic properties are found to be same calculated by LDA and GGA i.e; monomers and second-nearest-neighbor dimers are spin-polarized.

Chapter 5

Summary

5.1 Conclusions

Carbon nanomaterials have attracted much attention because they are candidates for post-silicon materials. Since carbon nanotubes (CNTs) were detected [10] and graphene was isolated from graphite [13], comprehensive studies have been carried out with the aim of exploiting the properties of these materials. In this study, we study two subjects. One is interlayer distance of the two-layer graphene and the other is atomic hydrogen adsorption in graphenes and CNTs.

In the study of first subject, we have carried out first principles DFT calculations using the LDA, and the VDWDFT to investigate the interlayer distance of the two-layer graphene. We found that the interlayer distance is the same as that of the graphite. The binding energy of the graphite was found to be larger than that of the two-layer graphene. The interlayer distance of the metastable AA stacking structure of the two-layer graphene is somewhat larger than that of the AB stacking structure. It is thus suggested that the interlayer distance becomes somewhat large when the stacking is deviated from the AB stacking. This deviation from the AB stacking is expected to occur in the case of double wall and multiwall carbon nanotubues since the two nearest neighbor tubes have different radii.

Nowadays, few layer graphenes are technologically important in semiconductor applications, due to gate control of the transport properties. Researchers have known that two-layer

graphene acts more like a semiconductor when immersed in an electric field. Now we also clarify layer distance by first-principles calculations. Therefore, our findings are very useful in the field of carbon nanomaterials as it can be used in semiconductor devices.

In the second subject, we study hydrogenation of carbon nanomaterials since hydrogen is a common impurity in graphenes and CNTs. We have performed first-principles calculations based on the spin-polarized GGA within density functional theory method . We studied the atomic hydrogen adsorption (monomers and dimers) in graphene, the armchair edge (5, 5) CNT, and the zigzag edge (10, 0) CNT. We found that the monomers are spin-polarized and have the magnetic moment of 1 μ_B. In the case of CNTs, the hydrogen atoms are located on the outer side of the CNTs. The binding energies in the CNTs (1.13 and 1.10 eV) are found to be much larger than that of graphene (0.53 eV). Therefore, the CNTs are easily hydrogenated compared with graphene.

In the most stable structures of the dimers in graphene and the CNTs, the two hydrogen atoms are bonded to the host carbon atoms which are nearest-neighbors. In the case of graphene, the two atoms are located on opposite sides. In contrast, in the cases of the armchair edge (5, 5) CNT and zigzag edge (10, 0) CNT, both hydrogen atoms are located on the outer side. When the two hydrogen atoms are bonded to the same sublattice of the host materials, the magnetic moment is found to be 2 μ_B in graphenes and the CNTs. We showed [in Figs. 4.5b and c] that the two hydrogen atoms are bonded to the carbon atoms (at the A sublattices in the graphene) which are the nearest-neighbor. The spin density appears at the hydrogen site and B sublattices. This result indicated that the hydrogen s-orbital is hybridized with the wavefunction at the Dirac cone. It is experimentally difficult to show the magnetic state in carbon nanomaterials by atomic hydrogen adsorption. Thus, the above mention results are very important in the field of carbon nanomaterial and hydrogenation of carbon materials is promising candidate of post-silicon materials.

Both interlayer distance of the two-layer graphene and atomic hydrogen adsorption in graphenes and CNTs are important in the field of carbon nanomaterials. Finally, we suggest that our findings open new possibility of carbon materials in the field of electronic devices.

5.2 Future Plan

We succeed to investigate the layer distance of the two-layer graphene. We clarify that the layer distance is the same as that of graphite. Previously, GGA calculation was performed on the graphite slabs in which small numbers of graphite sheets are stacked in ABAB fashion [67]. In the case of the odd numbered graphite slab, they found that layer distances are close to that of bulk graphite. On the other hand, in the case of even numbers of the slab, they found layer distances are greater than that of graphite. However, the validity of GGA is still questionable and layer distances of the few-layer graphenes are very important in the field of carbon nanomaterials. Therefore, our study is still insufficient. In future, we would like to investigate the layer distances of few-layer graphenes (up to seven slabs) by using VDWDFT.

In the case of atomic hydrogen adsorption in carbon material, we clarify most stable structures of monomers and dimers. However, most stable structures of trimmer, tetramer and so on are still unclear. As hydrogenation in carbon material is promising way for hydrogen storage, and it is very important in the field of nanomaterial. So, next we will clarify most stable structures of graphene (multilayer-graphene) by atomic hydrogen adsorption by increasing the number of hydrogen atoms. We will show the relation between the number of hydrogen atoms and binding energies per hydrogen atom. We will also clarify STM images of those structures.

Our future study will be very important in the field of carbon materials. Moreover, we can be able to predict the properties of the materials which do not exist in nature and design new materials.

Appendix A

van Der Waals Density Functional theory (VDWDFT)

PHASE [49] can calculate total energies and electronic states, including the van der Waals (vdW) interaction. In this appendix, we explain the function used for the vdW term. The vdW interaction is calculated by a nonempirical method. It is based on the VDWDFT given by Dion et al. [62] As we know conventional DFT (LDA and GGA) is usually insufficient to include van der Waals interaction, which is prominent in weakly bonded materials such as molecular crystal and many organic compounds [68, 69, 70]. Since the layer interaction is of the van der walls type, therefore, GGA cannot be used for systems in which the vdW interaction makes a large contribution. As the function contains no experimental parameters; thus, it is appropriate for any type of system.

Phase software can able to calculate the nonlocal correlation term E_c^{nl} (i.e., the vdW term) and the local correlation term E_c^{LDA}. The total exchange-correlation term, including the vdW interaction, is obtained by adding the local and nonlocal terms to the GGA exchange term. Thus, the total exchange-correlation energy is expressed by:

$$E_{xc} = E_x^{GGA} + E_c^{LDA} + E_c^{nl} \tag{A.1}$$

The third term on the right hand side of Eq. (A.1) is the most difficult to calculate. This is

what we call the van der Waals interaction; to calculate this term, we use the VDWDFT given by Dion et al. [62]. They write E_c^{nl} as

$$E_c^{nl} = \frac{1}{2}\int d\mathbf{r_i}\mathbf{r_k}\rho(\mathbf{r_i})\phi(\mathbf{r_i},\mathbf{r_k})\rho(\mathbf{r_i}) \tag{A.2}$$

Equation A.2 contains two spatial variables: $\mathbf{r_i}$ and $\mathbf{r_k}$. This means that Eq. A.2 considers nonlocal interactions between electron densities at points $\mathbf{r_i}$ and $\mathbf{r_k}$. This is the main difference between Eq. A.2 and the formula used in GGA and LDA. The function containing these two variables, $\phi(\mathbf{r_i},\mathbf{r_k})$, is given by

$$\phi(\mathbf{r_i},\mathbf{r_k}) = \frac{2}{\pi^2}\int_0^\infty dadba^2b^2WT \tag{A.3}$$

Here

$$\begin{aligned} W(a,b) &= \frac{2}{a^3b^3}[(3-a^2)bcosbsina + (3-b^2)acosasinb \\ &\quad +(a^2-b^2-3)sinasinb - 3abcosacosb] \end{aligned} \tag{A.4}$$

and

$$\begin{aligned} &T[x_i(a),x_i(b),x_k(a),x_k(b)] \\ &= \frac{1}{2}\left[\frac{1}{x_i(a)+x_i(b)} + \frac{1}{x_k(a)+x_k(b)}\right] \\ &\quad \times\left[\frac{1}{(x_i(a)+x_k(a))(x_i(b)+x_k(b))} + \frac{1}{(x_i(a)+x_k(b))(x_i(b)+x_k(a))}\right] \end{aligned} \tag{A.5}$$

The remaining variable is given by

$$x_j(a) = \frac{a^2}{2}\times\frac{1}{1-exp\left(-\frac{4\pi a^2}{9d_j^2}\right)}, \tag{A.6}$$

where

$$d_j = |\mathbf{r_i}-\mathbf{r_k}|q_0(\mathbf{r_j}), \tag{A.7}$$

where

$$q_0(\mathbf{r_j}) = -\frac{4\pi}{3}\epsilon_{xc}^{LDA}\rho(\mathbf{r_j}) - \frac{Z_{ab}}{9}\left[\frac{\nabla\rho(\mathbf{r_j})}{2k_F(\mathbf{r_j})\rho(\mathbf{r_j})}\right]^2 k_F(\mathbf{r_j}) \tag{A.8}$$

where

$$k_F^3 = 3\pi^2\rho(\mathbf{r_j}), (j = i\ or\ k) \tag{A.9}$$

The coefficient $Z_{ab} = -0.8491$ is determined by a first-principle calculation, and it does not change with a change in system. From these equations, we can see that the electron density $\rho(\mathbf{r})$ is the only input data to the functional $\phi(\mathbf{r_i}, \mathbf{r_k})$. The quantity ϵ_{xc}^{LDA} in Equ. A.8 is the exchange-correlation energy density in LDA. These formulas are based on the plasmon-pole model, and because of this, the vdW interaction can be obtained with a relatively low computational cost.

Appendix B

Hydrogen Adsorbed in Two-layer graphene

B.1 Results and Discussions

We clarify hydrogen monomer and dimers in mono-layer graphene. However, hydrogenation in multi-layer graphene is still not clear. In this appendix, we report hydrogen monomer and dimers in two-layer and three-layer graphenes.

Here firsy we construct a two-layer graphene having AB stacked fashion where the layer distance is 3.35 Å [Figs.B.1(a,c)]. Next we carry out calculations of hydrogen monomers on upper layer of two-layer graphene (B stacking). In the most stable geometry the hydrogen atom is located on the outer side of the two-layer graphene and the atom is bonded to one carbon atom [Fig. B.1]. The geometry where the hydrogen atom is located inner side the two-layer graphene.[Fig.B.1 (b)] has 0.05 eV higher energy than that of most stable geometry[Fig.B.1(a)]. In the most stable geometry [Fig. B.1(a,c)] the bond angle of H-C1-C2 is 101.3 ° compared with 99.4 ° in the metastable structure [Fig.B.1(b,c)] and this bond angle which is close to monomer on graphene(102.3 °). Therefore, the bond angle in the most stable geometry is close to the sp^3 bond angle. The bond length between the hydrogen atom and nearest-neighbor carbon atom for most stable structure and metastable structures are 1.14 Å and 1.16 Å respectively. The most

stable and metastable geometries are found to be spin-polarized and have a magnetic moment of 1 μ_B. As shown in Fig. B.2 the spin density appears at the same stacking where the hydrogen atom is boned and the spin density is located at the hydrogen site and at the nearest and third-nearest-neighbors of the carbon atom where the hydrogen is bonded. This spin distribution is similar to that of the graphene [Fig. 4.5(a)]. No spin density appears at the A stacking in which hydrogen atom is not boned. The binding energy of the most stable geometry is 1.11 eV.[Table B.1] which is same as that of graphene [Table 4.2].

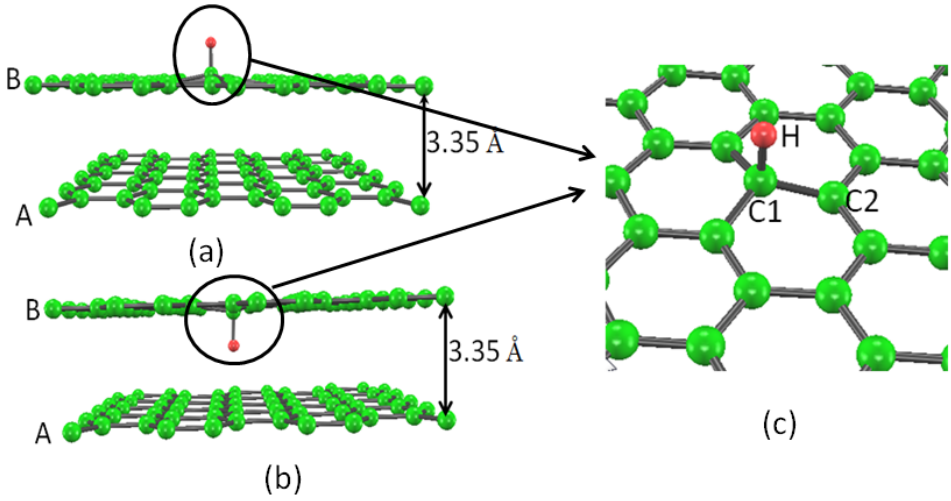

Figure B.1: Geometrical configuration of the hydrogen monomer in the two-layer graphene.

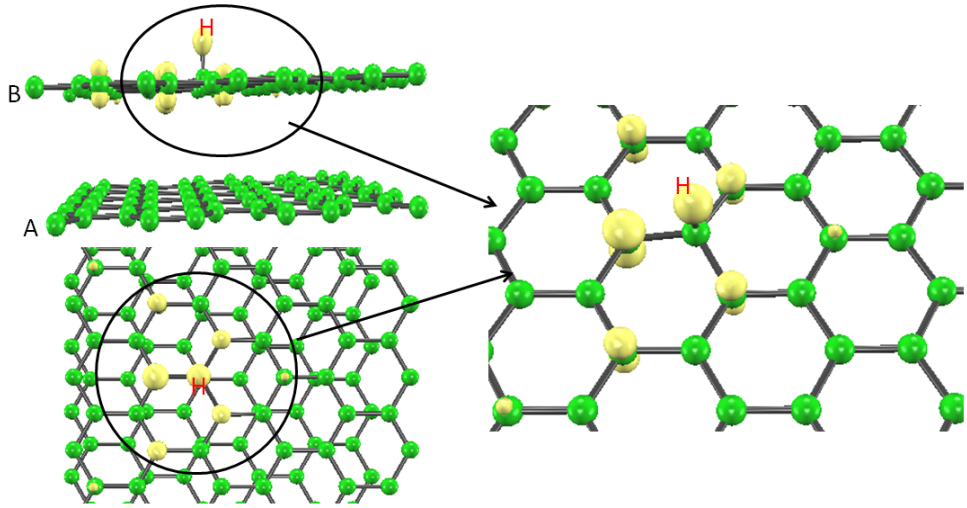

Figure B.2: Spin density distribution of hydrogen monomer in the two-layer graphene [Fig. B.1(a)]. The isosurface value is 0.005 $(a.u)^{-3}$.

Next, we carry out calculations of the hydrogen dimer in two-layer graphene. In the most stable geometry of the dimer, both hydrogen atoms are bonded to carbon atoms which are nearest-neighbors. The two hydrogen atoms are located on opposite sides [Fig. B.3(a)]. We find that the C1-C2 bond length [Fig. B.3(a)] is 1.51 Å and the bond angle of H1-C1-C2 [Fig. 4.2(a)] is 107.0° .These bond length and bond angle are close to dimer on graphene [sects. 4.1.1 and 4.1.2]. And also The bond length is close to the sp^3 bond length (1.54 Å) in diamond and the bond angle is close to the sp^3 bond angle (109.5°).

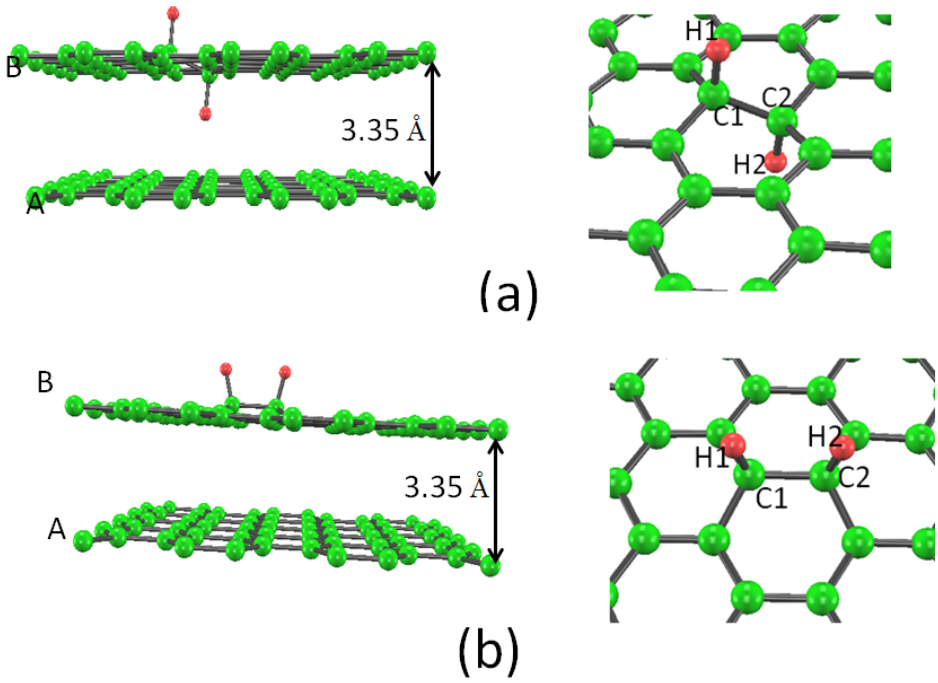

Figure B.3: Nearest-neighbor geometrical configurations of the hydrogen dimers in two-layer graphene

We find that the geometry where the two hydrogen atoms are located on the same side [Fig. B.3b)] has 0.60 eV higher energy than that of the most stable geometry. This energy difference is same as (0.60 eV) as described in sect. 4.1.1 and close to that of sect. 4.1.2. The calculated bond angle of H1-C1-C2 [Fig. 4.2(b)] in the metastable geometry is 103.8°, which somewhat deviates from the sp^3 bond angle. As a result, the C1-C2 bond length (1.54 Å) is longer than that (1.51 Å) of the most stable geometry. Therefore, it is expected that the higher energy of the metastable geometry is due to the deviation from the sp^3 hybridization.

The binding energy per hydrogen atom (E_b) Eq. (2.89) of the most stable geometry of the dimer is calculated to be 1.90 eV [Table B.1] which is close that of monolayer graphene [Table 4.2] and much bigger than that of monomer on graphene (1.14 eV) Table. 4.2, Therefore, the every cases the dimer is much more stable than the monomer. The same result also found in sect. 4.1.

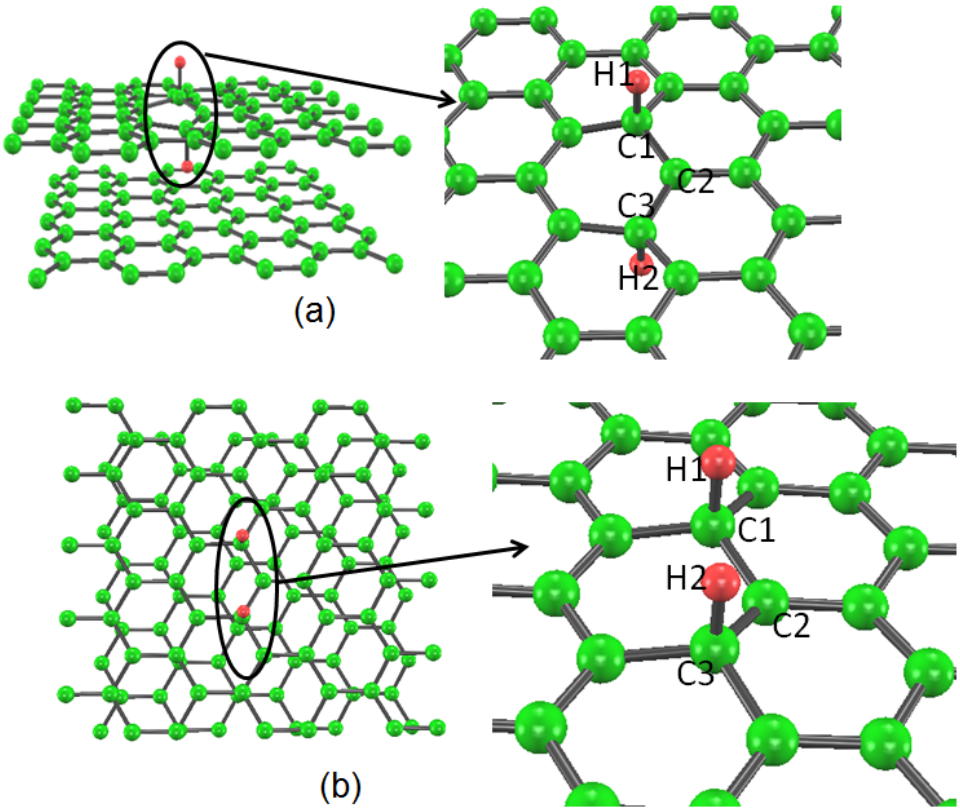

Figure B.4: Second-nearest-neighbor geometrical configuration of the hydrogen dimers in two-layer graphene.

Table B.1: Hydrogen monomers and dimers in two-layer graphene and three-layer graphene. NN and SN denote the nearest-neighbor and second-nearest-neighbor configurations, respectively. E_b is the bindining energy per hydrogen atom. These results are based on the LSDA calculations.

	Position	Geometry Figure number	C-H bond length (Å)	Avg. H-C-C bond angle (°)	E_b eV	Magnetic moment μ_B
Two-layer graphene	Monomer	B.1(a)	1.14	102.3	1.11	1
		B.1(b)	1.16	99.4	1.06	1
	NN dimers	B.3(a)	1.13	107.03	1.90	0
		B.3(b)	1.12	103.8	1.61	0
	SN dimers	B.4(a)	1.14	103.7	1.13	2
		B.4(b)	1.15	102.2	1.07	2
Three-layer graphene	Monomer	–	1.14	101.12	1.16	1
		–	1.16	99.13	1.12	1
	NN dimers	–	1.13	106.8	1.97	0
		–	1.12	104.0	1.65	0
	SN dimers	–	1.14	103.1	1.13	2
		–	1.15	103.1	1.09	2

Next, we study the case that the two hydrogen atoms are bonded to second-nearest-neighbor carbon atoms. The energy in the case that the two hydrogen atoms are located on opposite sides [Fig. B.4(a)] is 0.09 eV lower than that when the two hydrogen atoms are on the same side [Fig. B.4(b)] and 1.54 eV higher than that of the most stable geometry where the two hydrogen atoms are bonded to nearest-neighbor carbon atoms [Fig. B.3(a)]. This energy difference is close to that of GGA calculations 1.57 eV sect. [4.1.1 and 4.1.2]. The bond angle of H2-C3-C2 in Fig. B.4(a) is 103.6°, which is larger than that in Fig. B.4(b) (102.2 °). Therefore, the former angle

is closer to the sp^3 bond angle than the latter bond angle, which is expected to be the origin of the energetic stability of the former geometry.

Both geometries are found to be spin-polarized and have magnetic moments of 2 μ_B. As shown in Fig. B.5 the spin density appears at the same stacking where the hydrogen atom is boned (B stacking) and the spin density is located at the hydrogen site and at the nearest and third-nearest-neighbors of the carbon atom where the hydrogen is bonded. This spin distribution is similar to that of the graphene [Fig. 4.5(a)] and also monomer in two-layer graphene [sect.B.2]. No spin density appears at the A stacking in which hydrogen atom is not boned. The spin density distribution is same as shown in Fig. 4.5(b) and B.2, a large spin density is located at the hydrogen site and the two-layer graphene sublattice, which is different from the sublattice to which the hydrogen is bonded.

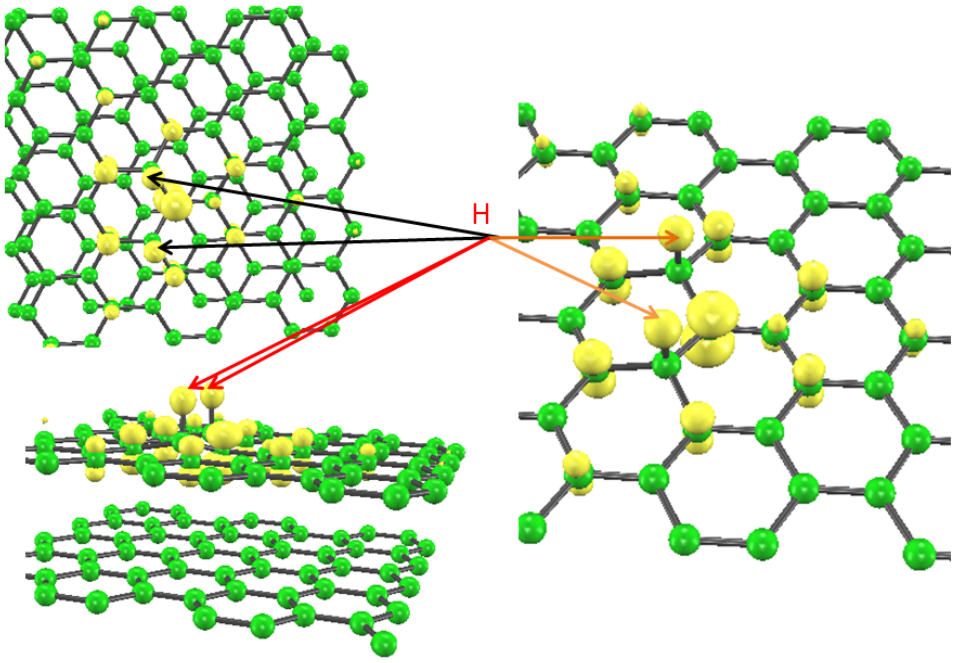

Figure B.5: Spin density distribution of hydrogen dimer having second-nearest-neighbor configuration [Fig. B.4(b)]in the two-layer graphene. The isosurface value is -0.01 $(a.u)^{-3}$.

We also carry out calculations of hydrogen monomers and dimers in three-layer graphene.

We find that the effect of hydrogenation is similar to that of mono-layer graphene. We tabulate the information of binding energies, bond angles and magnetizations based on the LSDA in Table B.1.

B.2 Conclusions

By using first-principles calculations based on the local spin Density approximation (LSDA) within the density functional theory method, we studied hydrogen monomers and dimers in two-layer graphene. We found that the monomers are spin-polarized and have magnetic moment 1 μ_B. The binding energies of the hydrogen monomer, and most stable dimer is 1.11 eV and 1.90 eV, respectively. Therefore, most stable dimer is much more stable than monomer. In the most stable structures of the dimers in two-layer graphene, the two hydrogen atoms are bonded to the host carbon atoms which are nearest-neighbors. Whereas, when the two hydrogen atoms are bonded to the same sublattice of the host materials, magnetic moments of 2 μ_B appear in two-layer graphene. We found that when the two hydrogen atoms are bonded to third-nearest-neighbor carbon atoms, the electronic structure is nonmagnetic.

References

[1] N. Hamada, S. Sawada, and A. Oshiyama, Phys. Rev. Lett. 68, 1579 (1992)

[2] Y. -W. Son, M. L. Cohen, and S. G. Louie, Nature 444, 347 (2006)

[3] O. Hod, V. Barone, and G. E. Scuseria, Phya. Rev. B 77, 035411 (2008)

[4] E. Kan, Z. Li, J. Yang, and J. G. Hou, J. Am. Chem. Soc. 130, 4224 (2008)

[5] A. F. Hebard, M. J. Rosseinsky, R. C. Haddon, D. W. Murphy, S. H. Glarum, T. T. M. Palstra, A. P. Ramirez, and A. R. Kortan, Nature 350, 600 (1991)

[6] K. Tanigaki, T. W. Ebbesen, S. Saito, J. Mizuki, J. S. Tsai, Y. Kubo, and S. Kuroshima, Nature 352, 222 (1991)

[7] P. -M. Allemand, K. C. Khemani, A. Koch, F. Wudl, K. Holczer, S. Donovan, G. GrNuner, and J. D. Thompson, Science 253, 301 (1991)

[8] M. Fujita, K. Wakabayashi, K. Nakada, and K. Kusakabe, J. Phys. Soc. Jpn. 65, 1920 (1996)

[9] S. Okada, and A. Oshiyama, J. Phys. Soc. Jpn. 72, 1510 (2003)

[10] S. Iijima: Nature (London) **354** (1991) 56.

[11] N. R. Wilson and J. V. Macpherson, Carbon nanotube tips for atomic force microscopy: Nature Nanotechnology, **4** 483 (2009)

[12] A. L. Chun, Nanomaterials: Carbon meets cotton: Nature Nanotechnology, June 2008.

[13] K.S. Novoselov, A.K. Geim, S.V. Morozov, D. Jiang, Y. Zhang, S.V. Dubonos, I.V. Grigorieva, and A.A. Firsov: Science **306** (2004) 666.

[14] M. Koshino, and T. Ando: . Solid State Commun. **149**, 1123 (2009).

[15] C. H. Lui, et al. Nano Lett. **11**,164 (2010).

[16] W. Zhu, V. Perebeinos, M. Freitag, and P. Avouris: . Phys.Rev. B **80**, 235402 (2009).

[17] J. T Ye,. et al. A ; Proc. Natl Acad. Sci. USA **108**, 13002 (2011)

[18] H. Min, B. Sahu, S. K. Banerjee, and A. H. MacDonald: Phys. Rev. B **75** (2007) 155115.

[19] E. McCann and V.I. FalE'ko: Phys. Rev. Lett. **96** (2006) 086805.

[20] E. McCann: Phys. Rev. B **74** (2006) 161403(R).

[21] Y. Zhang, T-T, Tang, C. Girit, M. C. Martin, A. Zettl, M. F. Crommie, Y. R. Shen, and F. Wang: Nature (London) **459** (2009) 820.

[22] J. B. Oostinga, H. B. Heersche, X. Liu, A. F. Morpurgo, and L. M. K. Vandersypen: Nature Mater. **7** (2008) 151.

[23] K. F. Mak, C. H. Lui, J. Shan, and T. F. Heinz: Phys. Rev. Lett. **102** (2009) 256405.

[24] A. Ranjbar, M. Khazaei, M. S. Bahramy, H. Mizuseki, and Y. Kawazoe: Phys. Rev. B **82** (2010) 165446.

[25] M. Khazaei, M. S. Bahramy, A. Ranjbar, H. Mizuseki, and Y. Kawazoe: Carbon **47** (2009) 3306.

[26] T. Roman, W. A. Dinõ, H. Nakanishi, and H. Kasai: J. Phys. Soc. Jpn **76** (2007) 114703.

[27] Y. Miura, H. Kasai, W. A. Dinõ, H. Nakanishi, and T. Sugimoto: J. Phys. Soc. Jpn **72** (2003) 995.

[28] E. J. Duplock, M. Scheffler, and P. J. D. Lindan: Phys. Rev. Lett. **92** (2004) 225502.

[29] E. C. Lee, Y.-S. Kim, Y.-G. Jin, and K. J. Chang: Phys. Rev. B **66** (2002) 073415.

[30] S. P. Chan, G. Chen, X. G. Gong, and Z. -F Liu: Phys. Rev. Lett. **87** (2001) 20.

[31] Y. Ma, P. O. Lehtinen, A. S. Foster, and R. M. Nieminen: Phy. Rev. B **72** (2005) 085451.

[32] O. Gülseren, T. Yildirim, and S. Ciraci: Phys. Rev. B **68** (2003) 115419.

[33] D. W. Boukhvalov, M. I. Katsnelson, and A. I. Lichtenstein: Phys. Rev. B **77** (2008) 035427.

[34] Y. Ferro, D. Teillet-Billy, N. Rougeau, V. Sidis, S. Morisset, and A. Allouche: Phys. Rev. B **78** (2008) 85417.

[35] Y. Lei, S. A. Shevlin, W. Zhu, and Z. X. Guo: Phys. Rev. B **77** (2008) 134114.

[36] A. Andree, M. L. Lay, T. Zecho, and J. Küpper: Chem. Phys. Lett. **425** (2006) 99.

[37] L. Hornekær, Ž. Šljivancanin, W. Xu, R. Otero, E. Rauls, I. Stensgaard, E. Lægsgaard, B. Hammaer, and F. Besenbacher: Phys. Rev. Lett. **96** (2006) 156104.

[38] L. Hornekær, E. Rauls, W. Xu, Ž. Šljivancanin, R. Otero, I. Stensgaard, E. Lægsgaard, B. Hammaer, and F. Besenbacher: Phys. Rev. Lett. **97** (2006) 186102.

[39] L. Hornekær, W. Xu, R. Otero, E. Lægsgaard, and F. L. Besenbacher: Chem. Phys. Lett. **446** (2007) 237.

[40] K. Nagatsu, S. Chiashi, S. Konabe, and Y. Homma: Phys. Rev. Lett. **150** (2010) 157403.

[41] S. S. Han, and H. M Lee: Carbon **42** (2004) 2169.

[42] S. Casolo, O. M. Lovvik, R. Martinazzo, and G. F. Tantardini: J. Chem. Phys. **130** (2009) 054704.

[43] X. Pei, X. Yang, and J. Dong: Phys. Rev. B **73** (2006) 195417.

[44] K. Nishida, N. Imaizumi, M. Irita, H. Kato, and Y. Homma: Appl. Phys. Express **4** (2011) 115102.

[45] J. Zhou, Q. Wang, Q. Sun, X. S. Chen, Y. Kawazoe, and P. Jena: Nano Lett. **9** (2009) 3867.

[46] A. K. Singh and B.I. Yakobson: Nano Lett. **9**, 1540 (2009)

[47] H. Sahin, C. Ataca, and S. Ciraci, Appl. Phys. lett. **95** 222510 (2009)

[48] N. S. Nurainun, J. Lin, M. S. Alam, K. Nishida, and M. Saito: Mater. Res. Soc. Jpn. **36** (2011) 619.

[49] http://www.ciss.iis.u-tokyo.ac.jp/.

[50] D. R. Hartree. *The wave mechanics of an atom with non-Coulombic central I, II, III,* volume 24:89,111,426. Proc. Cambridge Phil. Soc, 1928.

[51] P. Hohenberg, and W. Kohn: Phys. Rev. B **136** B864 (1964)

[52] W. Kohn and L. J. Sham Phys. Rev. 1133**A**:140,(1965)

[53] A. D. Becke, Phys. Rev. **A 38**, 3098 (1988).

[54] J. P. Perdew, J. A. Chevary, S. H. Vosko, K. A. Jackson, M. R. Pederson, and C. Fiolhais, Phys. Rev. **B 46**, 6671 (1992).

[55] J. P. Perdew and Y. Wang: Phys. Rev. B **46** (1992) 6671.

[56] J. P. Perdew, K. Burke, and M. Ernzerhof, Phys. Rev. Lett. **77**, 3865 (1996).

[57] Jorge Kohanoff. (2006). Electronic Structure Calculation for Solids and Molecules: Theory and Computational Methods (pp. 85-91). United Kingdom: Cambridge University Press.

[58] P. S. Svendsen and U. von Barth. (1996). Gradient expansion of the exchange energy from second-order density response theory. Phys. Rev. B 54, 17402- 17413.

[59] J. P. Perdew and K. Burke. (1996). Comparison shopping for a gradientcorrected density functional. Int. J. Quant. Chem. 57, 309-319.

[60] D. R. Hamann, M. SchlNuter, and C. Chiang: Phys. Rev. Lett., **43**, 1494, (1979)

[61] D. Vanderbilt: Phys. Rev. B**41** (1990) 7892(R).

[62] M. Dion, H. Rydberg, E. Schröder, D.C. Langreth, and B.I. Lundqvist: Phys. Rev. Lett.**92** (2004) 246401.

[63] M. Dion, H. Rydberg, E. Schröder, D.C. Langreth, and B.I. Lundqvist: Phys. Rev. Lett. **95** (2005) 109902.

[64] Y. Okamoto: J. Phys. Chem. A **105** (2001) 7634.

[65] S.Iijima: Chem. Scr. **14** (1978-79) 117.

[66] X. Sun, C.-H. Kiang, M. Endo, K. Takeuchi, T. Furuta, M.S. Dresselhaus: Phys. Rev. B **54** (1996) 12629.

[67] K.Yoshikawa, T. Yumura, T. Yamabe, and S. Bandow: J. Am. Chem. Soc. **122** (2000) 11871.

[68] P. Hobza, J. Sponer, and T. Resche: J. Comput. Chem. **16** (1995) 1315.

[69] S. Kristyan and P. Pulay: Chem. Phys. Lett. **229** (1994) 175.

[70] E. Ruiz, D.R. Salahub, and A. Vela: J. Am. Chem. Soc. **117** (1995) 1141.

[71] Y. Baskin and L. Meyer: Phys. Rev. **100** (1955) 544.

[72] S. Lebègue, J. Harl, T. Gould, J.G. Ángyán, G. Kresse, and J. F. Dobson: Phys. Rev. Lett. **105** (2010) 196401.

[73] Y. Omata, Y. Yamagami, K. Tadano, T. Miyake, and S. Saito: Physica E **29** (2005) 454 .

[74] E. Ziambaras, J. Kleis, E. Schröder, and P. Hyldgaard: Phys. Rev. B **76** (2007) 155425.

[75] D.C. Langreth, B.I. Lundqvist, S.D. Chakarova-Käck, V.R. Cooper, M. Dion, P. Hyldgaard, A. Kelkkanen, J. Kleis, L. Kong, S. Li, P.G. Moses, E. Murray, A. Puzder, H. Rydberg, E. Schröder, and T. Thonhauser: J. Phys.: Condens. Matter **21** (2009) 084203

[76] M. Hasegawa and K. Nishidate: Phys. Rev. B **70** (2004) 205431.

[77] S.B. Trickey, F. Muller-Plathe, G. H. F. Diercksen, and J. C. Boettger: Phys. Rev. B **45** (1992) 4460.

[78] M.C. Schabel and J.L. Martins: Phys. Rev. B **46** (1992) 7185.

[79] J.C. Charlier, X. Gonze, and J.P. Michenaud: Europhys. Lett. **28** (1994) 403.

[80] L.A. Girifalco and R.A. Ladd: J. Chem. Phys. **25** (1956) 693.

[81] R. Zacharia, H. Ulbricht, and T. Hertel: Phys. Rev. B **69** (2004) 155406.

[82] D. J. Chadi and K. J. Chang: Phys. Rev. B **38** (1998) 1523.

[83] T. Nagao, J. T. Sadowski, M. Saito, S. Yaginuma, Y. Fujikawa, T. Kogure, T. Ohno, Y. Hasegawa, S. Hasegawa, and T. Sakurai: Phys. Rev. Lett. **93** (2004) 105501.

[84] Y. Okamoto and Y. Miyamoto, J. Phys. Chem. B **105** , 3470 (2001).

[85] N. Jacobson, B. Tegner, E. Schroder, P. Hyldgaard, and B. I. Lundqvist, Comput. Mater. Sci. **24**, 273 (2002)

[86] A. Krasheninnikov, 2000, in: *Computational Methods for Material* Science, lecture notes, University of Helsinki

Acknowledgments

First of all, I would like to express the deepest appreciation to my supervisor Professor Mineo Saito for initiating this project, guidance, support and discussion as well as encouragement. I would like to express my gratitude to Professor Fumiyuki Ishii, Professor Tatsuki Oda,Professor Shinichi Miura, and Professor Hidemi Nagao for their kind support. I also wish to express grateful acknowledgment to the Staffs of the Graduate School of Natural Science and Technology, Kanazawa University for their care and help during the years I was studying here.

I would like to thank all members of the computational science research group at the Kanazawa University. In addition, I would like to thank my Bangladeshis colleagues and friends who helped me and gave moral support before I came here. However, because the list might be too long and by fear of leaving someone out, I will simply say thank you very much to you all.

I am forever indebted to my mom, my sisters and my brother for their boundless love, understanding, endless patience and encouragement. The financial support of the ”*Kanazawa University Special admission quota for graduate students from Designated Universities Special selection of the Enhancement of international Exchange Scholarship*” and Research Assistance are gratefully acknowledged.